Vibration Analysis of Piezoelectric Energy Harvesting Advanced Light Weight Rotating Beams

Ahmed Salih

Submitted to the
Institute of Graduate Studies and Research
in partial fulfillment of the requirements for the degree of

Master of Science
in
Mechanical Engineering

Eastern Mediterranean University
June 2022
Gazimağusa, North Cyprus

Approval of the Institute of Graduate Studies and Research

Prof. Dr. Ali Hakan Ulusoy
Director

I certify that this thesis satisfies all the requirements as a thesis for the degree of Master of Science in Mechanical Engineering.

Assoc. Prof. Dr. Murat Özdenefe
Chair, Department of Mechanical Engineering

We certify that we have read this thesis and that in our opinion it is fully adequate in scope and quality as a thesis for the degree of Master of Science in Mechanical Engineering.

Asst. Prof. Dr. Babak Safaei
Supervisor

Examining Committee

1. Prof. Dr. Qasim Zeeshan
2. Assoc. Prof. Dr. Shaban Ismael Albrka
3. Asst. Prof. Dr. Babak Safaei

ABSTRACT

Renewable energy is energy that can be found in nature as solar energy and wind energy. A new type of renewable energy is added recently: energy harvesting. This category is only for small systems such as sensors and one of its categories is vibrational energy. Material that gives the ability to convert mechanical energy (i.e. Vibration) to electrical energy and vice-versa is the piezoelectric material. In this thesis, a sandwich structure consisting of a piezoelectric layer and light materials is proposed, this structure can be inserted in different rotational environments such as flex plates tires, and the blade of a wind turbine, the vibration of these environments can be transformed to electrical energy to power sensors or any low power type of equipment. PZT-5H piezoelectric material will be used, the harmonic analysis will be applied to three different light materials to determine the voltage output from the PZT-5H which are aluminum and magnesium and, titanium. Noise will be added to the beams to enhance the output power of the harvesters and to make the systems have more than one stable position to allow the stochastic resonance phenomenon to occur. The temperatures on the produced electrical power will be also examined for each beam, the harmonic analysis will be done with the finite element method (FEM) on ABAQUS® software, curve fitting temperature data to get the elasticity at a desired temperature and noise inheritance are done using MATLAB® Software. The results showed that Magnesium substrate produced the highest electrical power by 756.06 μW and Titanium substrate comes next with 501.9 μW and at last Aluminum substrate with a value of 489.92 μW, also the results demonstrated that the temperature reduced the electrical power by overall but the highest substrate material was Aluminum with a

value of 427.0 μW and next comes the Magnesium substrate with a value of 401.0 μW and at last Titanium substrate with a value of 395.0 μW.

Keywords: Stochastic resonance, Finite element method, Euler-Bernoulli beam, Piezoelectric energy harvesting.

ÖZ

Yenilenebilir enerji, doğada güneş enerjisi ve rüzgar enerjisi olarak bulunabilen enerjidir. Son zamanlarda yeni bir yenilenebilir enerji türü eklendi: enerji hasadı. Bu kategori sadece sensörler gibi küçük sistemler içindir ve kategorilerinden biri de titreşim enerjisidir. Mekanik enerjiyi (yani Titreşim) elektrik enerjisine veya tam tersine dönüştürme yeteneği veren malzeme piezoelektrik malzemedir. Bu tezde, bir piezoelektrik katman ve hafif malzemelerden oluşan bir sandviç yapı önerilmiş, bu yapı esnek plaka katmanları ve bir rüzgar türbininin kanadı gibi farklı dönme ortamlarına yerleştirilebilmekte, bu ortamların titreşimi dönüştürülebilmektedir. sensörlere veya herhangi bir düşük güçlü ekipman tipine güç sağlamak için elektrik enerjisi, PZT-5H piezoelektrik malzeme kullanılacak, PZT-5H'den gelen voltaj çıkışını belirlemek için üç farklı hafif malzeme üzerinde harmonik analiz uygulanacaktır, bunlar alüminyum ve magnezyum ve Biçerdöverlerin çıkış gücünü artırmak ve sistemlerin stokastik rezonans olgusunun oluşmasına izin vermek için birden fazla kararlı konuma sahip olmasını sağlamak için kirişe titanyum gürültüsü eklenecek, Üretilen elektrik gücü üzerindeki sıcaklığın etkisi de her kiriş için incelenecektir, Harmonik analiz, ABAQUS® yazılımı üzerinde sonlu elemanlar yöntemi (FEM) ile yapılacaktır, elastisiteyi elde etmek için eğri uydurma sıcaklık verileri MATLAB® Yazılımı kullanılarak istenen bir sıcaklık ve gürültü mirası elde edildi, sonuçlar Magnezyum substratın 756.06 µW ile en yüksek elektrik gücünü ürettiğini ve Titanyum substratın 501.9 µW ile ardından geldiğini ve son olarak Alüminyum substratın 489.92 µW değerinde olduğunu gösterdi, ayrıca sonuçlar sıcaklığın elektrik gücünü genel olarak azalttığını, ancak en yüksek substrat malzemesinin 427,0 µW değerinde Alüminyum olduğunu ve ardından 401,0 µW değerinde Magnezyum substrat ve son olarak 395,0 μW değerinde Titanyum substrat olduğunu gösterdi.

Anahtar Kelimeler: Stokastik rezonans, Sonlu elemanlar yöntemi, Euler-Bernoulli ışını, Piezoelektrik enerji hasadı.

DEDICATION

To my Family

ACKNOWLEDGMENT

I would like to strongly acknowledge my dear supervisor Assist. Prof. Dr. Babak Safaei for support and advice and his help and continued guidance during this journey, if it wasn’t for him this work won’t be done, I am truly grateful for him.

TABLE OF CONTENTS

LIST OF TABLES

LIST OF FIGURES

Chapter 1

INTRODUCTION

1.1 Background

Piezoelectric materials are materials that generate electrical potential once a mechanical deformation is applied to it. The opposite case is also possible where if an electrical potential is applied to the material will show mechanical deformation depending on where the electrical potential is applied [1]. Many materials exhibit piezoelectric behavior such as quarts which is a crystal material. PZT which stands for lead zirconate titanate which has different types with different properties lithium niobate/tantalate, relaxor ferroelectrics, Polyvinylidene fluoride (PVDF). This material is used in one of two applications, the first one is as an actuator where the mechanical deformation does generate some kind of mechanical motion which would be useful, the second application is as a sensor where the produced electrical energy is used to power sensors which makes it perfect alternative for traditional batteries [2].

1.2 Problem Statement

The probelm that the thesis is trying to overcome is desgning a piezoelectric energy harvester beam that maximize the produce delecrical power and minimize the deformation happend to the beam during vibration.

1.3 Scope of the Thesis

The scope of this thesis is within energy harvesting, specifically in harvesting energy from relative motion using piezoelectric effect, also the scope include vibration behavior simulation using finite element method using ABAQUS® software.

ABAQUS® is selected since is gives the control over mesh configuration and element formulation since most other packages automate the element formulation selection and mesh configuration. Substrates selected for the three beams are aluminum and magnesium and titanium, the selected piezoelectric material was PZT-5H. The limitations of this research include the need of an experimental validation for finite element formulation for the three beams and also conducting a multiphysics simulation regarding the temperature effect on the three beams which requires high computational power.

1.4 Objectives of the Thesis

This work aims to perform a comparative study on three cantilever sandwich structures consisting of a piezoelectric layer and two substrate layers made of light metals. The aim is to optimize the maximum deformation that could occur to the structure due to the vibration, and the maximum amount of electrical voltage produced due to vibration, to give the ability to operate multiple sensors from one structure. PZT-5H will be the chosen material since it has the maximum electrical productivity compared to other piezoelectric materials. Vibration analysis is done on each beam to obtain the output power from vibration for each beam, and also temperature will be applied on each beam to see the power output for each beam.

1.5 Thesis Contribution

Electrical energy is highly desirable in range of applications and also an efficient electrical source that supplies enough electrical energy as demanded. in vibrational energy harvesting the structure that will transfer the vibrations and convert them into electrical energy should be sufficient to supply the sensors with enough energy to function properly.

The main contributions of this thesis are the following :

- Proposal of a methodology for designing the piezoelectric beam to optimize the electrical output and protect the beam from destruction due to vibration.
- Conducting vibration analysis on thr proposed desgin to observe the output power.
- Applying temperature on the proposed design to observe the output power from it.
- Validating the result with the related literature.

1.6 Thesis Outline

This thesis is divided into five chapters, the first chapter is the introduction to the thesis itself and the aim of the thesis. The second chapter will give a comprehensive literature review of the recent developments regarding the topic. The third chapter will be about the followed methodology in this thesis and material selection and beam design and the tool used for computation. The fourth chapter will demonstrate the results and compare it to the related literature and validate the result against relevant experimental data from literature. The fifth chapter will conclude the thesis.

1.7 Summary of the Chapter

To conclude, chapter one gave background information about piezoelectric energy harvesting, then the problem statement that gave the motivation to write this thesis and the main contributions from the thesis to overcome the statment problem are given and discussed, lastly the full thesis outline was illustrated where each chapter was summarized and explained including the conclusion of the whole thesis, chapter one was a full introduction to the field of the thesis and the thesis its self.

Chapter 2

LITERATURE REVIEW

This chapter is going to provide theoretical and background information regarding energy harvesting and its categories and background information about techniques used to analyze vibrational energy harvesting. A comprehensive review of piezoelectric energy harvesters in rotating environments is presented, in this review, the research papers will be classified into two types of vibrational excitations which are inertial and magnetic. The simulation techniques structural designs are going to be illustrated.

2.1 Energy Harvesting

Energy harvesting is a branch of renewable energy which is defined as the process of collecting energy from the environment, the type of energy that would be otherwise wasted as heat, the output energy is used to operate small systems such as wireless sensors and regular sensors which are the type of devices that rely on batteries to consume electrical energy. Energy harvesting has relay on five recourses of energy to convert to electrical energy which they are relative motion or vibration, Temperature gradient, light, electromagnetic radiation, chemical energy, each use a different type of material. The material associated with are summarized in Figure 1 [3].

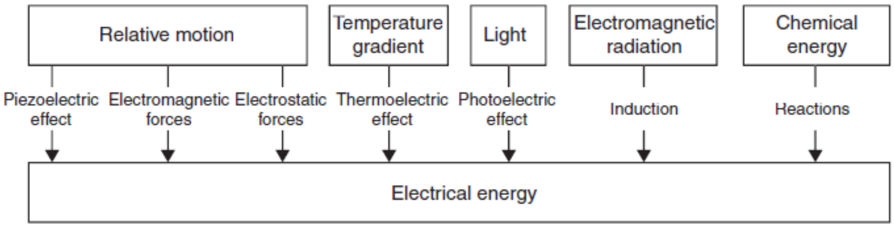

Figure 1: Categories of energy harvesting [5]

2.1.1 Piezoelectric Energy Harvesting

Piezoelectric material's special microstructure is the main cause for the piezoelectric effect, where if a mechanical deformation occurs the electrical potential inside the microstructure will differ creating a potential difference hence voltage. The reverse case is true where if a voltage is applied to the piezoelectric material a magnetic field starts to develop and producing magnetic force to deform the piezoelectric material. The polarity of the electrical potential depends on wither the load is tension or compression where for tension deformation the potential is positive and if the deformation was compression then the electrical potential is negative. The deformation depends on the polarity of the applied electrical potential where if the applied electrical potential is positive the piezoelectric material will deform in tension and if the applied electrical potential is negative the piezoelectric material will deform in compression due to the magnetic force generated from the microstructure. There are many materials which exhibit piezoelectric effect but the popular one is lead zirconate titanate, this material has very high electrical conductivity which is conserved in a very large range of temperatures making a perfect choice for many application [3]. Piezoelectric materials are not employed alone it is often supported with thick beams to form a sandwich beam. The stiffness of the supporting material with respect to the stifness of the piezoelectric material is a very important factor to improve the efficiency of the beam. Some of the material used to support the piezoelectric material are aluminum and brass ans steel. In litrature aluminum happnes to be the best choice sinc it is the lightest among other materials and tus posting the effecitiny of the structure. Sandwich beams which has piezoelectric material are mainly used in vibration application to caluclate the recounance frequancy of the beam and apply the relative damping to protect the strucutre and output the maximum power possible [4].

2.2 Inertial Excitation

This term refers to the effect of the environment's centrifugal force on a mounted cantilever beam with a proof mass at the free end. Inertial excitation is categorized into three types based on the location of the fixed end of the beam: softening inertial excitation, stiffening inertial excitation, and axial beam excitation.

2.2.1 Softening Inertial Excitation

When the fixed end of a cantilever beam is oriented toward the center of rotation and perpendicular to the rotation axis, this is referred to as a softening effect configuration, also known as an inward beam configuration. Some of the researchers who used this technique combined impact vibration with centrifugal excitation with various structural designs, while the rest only used centrifugal excitation. For example, Zhang et al. [5]. Reported a piezoelectric sandwich structure inside a wind turbine, the vibration was caused by centrifugal force and the impact of the beam on the turbine walls. Two configurations were developed (please see Figure 2), the finite element approach was used in the simulation, and it was compared to the generated analytical model for the system to determine the voltage output as a function of excitation frequency, which represents the wind speed. In the simulation results shown in Figure 4 the voltage showed a peak voltage of 30.0 volts approximately at an excitation frequency of 98.0 Hz which is the threshold of the system after this frequency the voltage begins to drop down significantly. As for experimental work the wind blowing on the harvester was simulated using a wind tunnel so the wind can go through and hit the harvester in the center as shown in Figure 3, the output voltage was measured via oscilloscope and the wind speed were measured via anemometer. The experimental results shown in Figure 5 the second configuration outputted far superior voltage then the first configuration since there are three beams inside the turbine in the second configuration. Figure 5 shows that if the wind speed reached a certain value the voltage starts to decrease with the increase of wind speed, that due to the inability of the harvester to change position before the next impact strikes. In the first configuration the peak voltage was 160.2 V at the threshold of 14 m/s and for the second configuration the peak voltage of 24.0 V at threshold of 10 m/s.

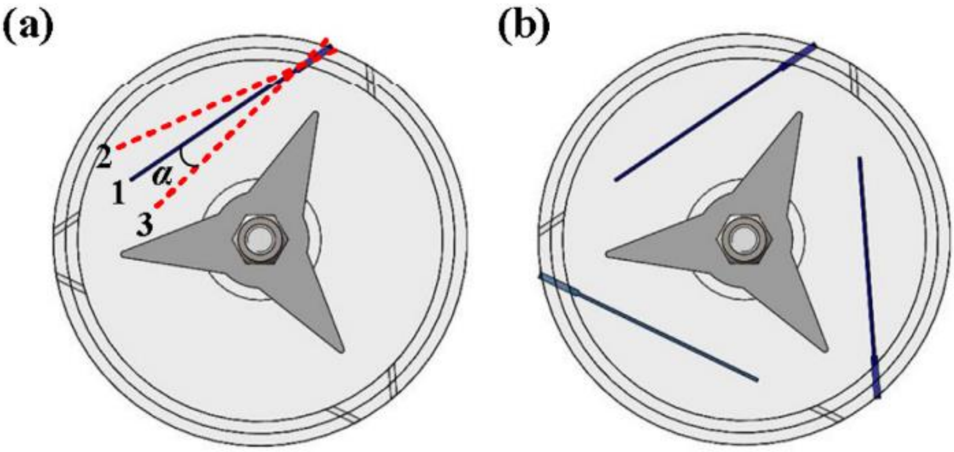

Figure 2: On the left is the first configuration and on the right, the second configuration [5]

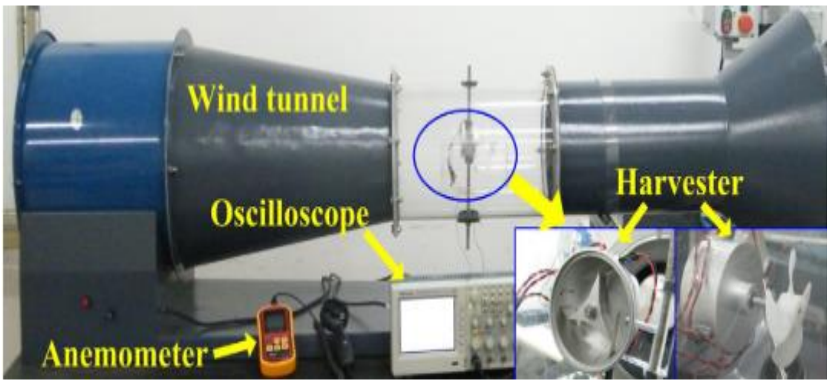

Figure 3: Experimental setup [5]

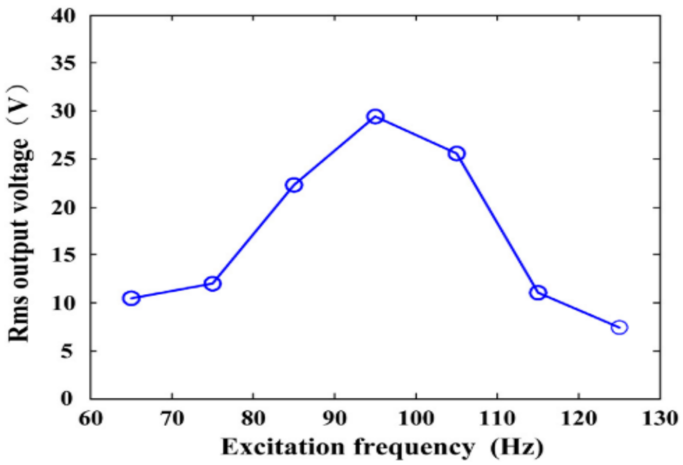

Figure 4: Simulation results: Voltage output VS excitation frequency [5]

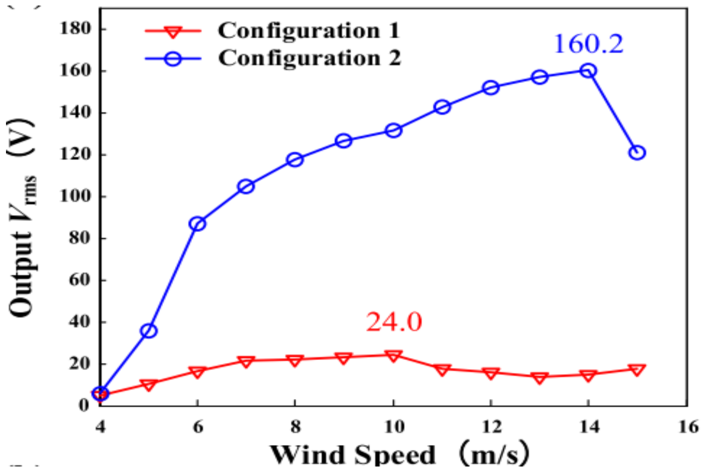

Figure 5: Experimental results [5]

Another report was from Rui et al. [6]. Who developed a multi-beam configuration that includes a piezoelectric sandwich structure and a low excitation beam that delivers an impacting force to the piezoelectric beam in addition to the centrifugal force applied to the beam. As well as a limiting protection beam that, as the name implies, protects the impacting beam from over deforming while in vibration (please see Figure 6). Two configurations were developed out of the proposed system, the first is a softened configuration and the other one was hardened configuration. Lumped parameter principle was employed to derive the governing equation for both systems. The experimental validation was carried out inside a vibration isolation system where the harvester with installed on a desk and the disk was attached to a servo motor. The produced voltage was measured using data acquisition system which later will be transmitted into a computer device, the experimental setup is shown in Figure 7.

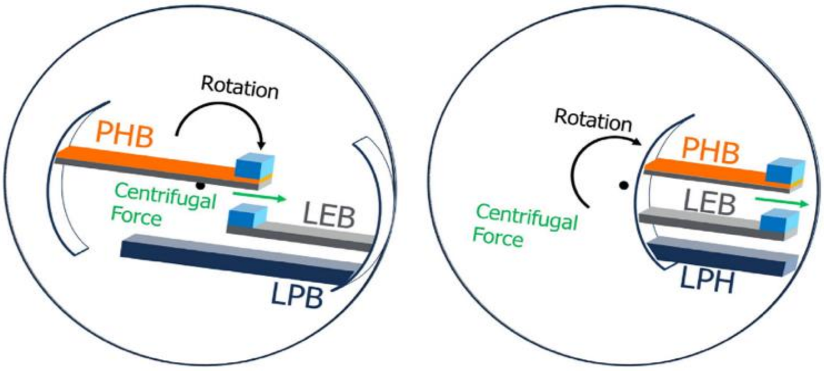

Figure 6: On the left is the softened configuration and on the right is the hardened configuration [6]

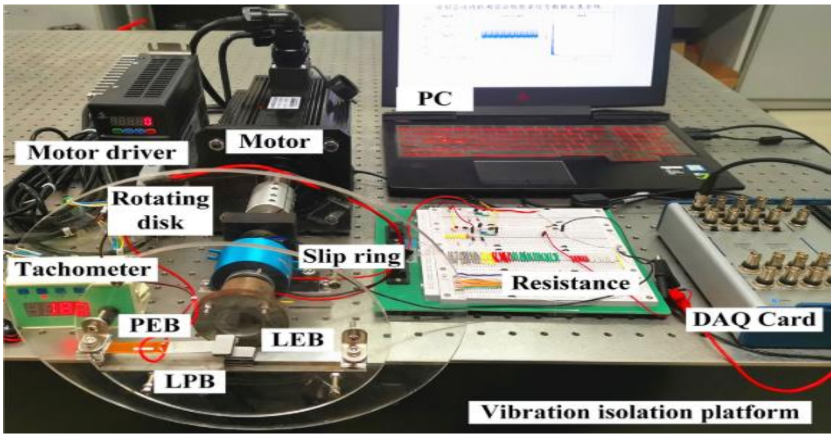

Figure 7: Experimental setup [6]

The output voltage was measured across a load of 610 kΩ. The simulation results and experimental result comparison are shown in Figure 8 in form of curve fitting. The simulation results showed a relatively good fit but there was a noticeable error at the first impact of the beam but the rest of the graph showed remarkable accuracy. Regarding the non-impact softening configuration, all researchers who used this configuration used a relatively similar configuration, which is a cantilever beam with a proof mass attached at the free end, which is a cantilever beam is placed in a rotational environment as illustrated in Figure 9. Most of the researches used different piezoelectric materials and derived the governing ordinary differential equation and solved these equations numerically. The boundary condition was gravitational excitation, which was represented as periodic sine excitation with an amplitude equal to the gravitational force, and the typical tool used for this purpose was MATLAB® ordinary differential equation solvers. Figure 9 depicts the beam configuration used by various researchers; however, the material, rotational environment, and analysis techniques vary slightly differ from researcher to researcher. For example, Guan et al. [7]. Presented an analytical model to predict the peak voltage of the piezoelectric material and validated his theoretical results experimentally. The experimental setup was composed of an AC motor and a full bridge rectifier, and an oscilloscope.to measure the voltage produced out of the harvester. The experimental setup is shown in Figure 10 and the zoomed-in version where the harvester is illustrated inside the AC motor is shown in Figure 11. The results of the simulation and the experiment are shown in Figure 12, the results showed the proportional relationship between the output powers although the error is considerable.

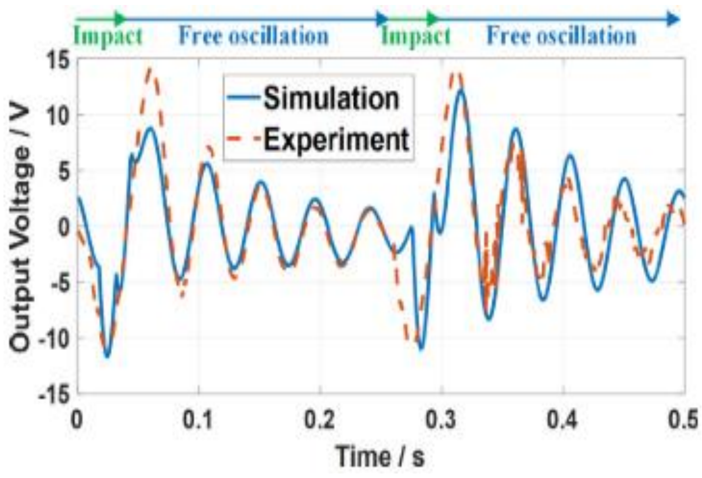

Figure 8: Simulation and experimental results comparison [6]

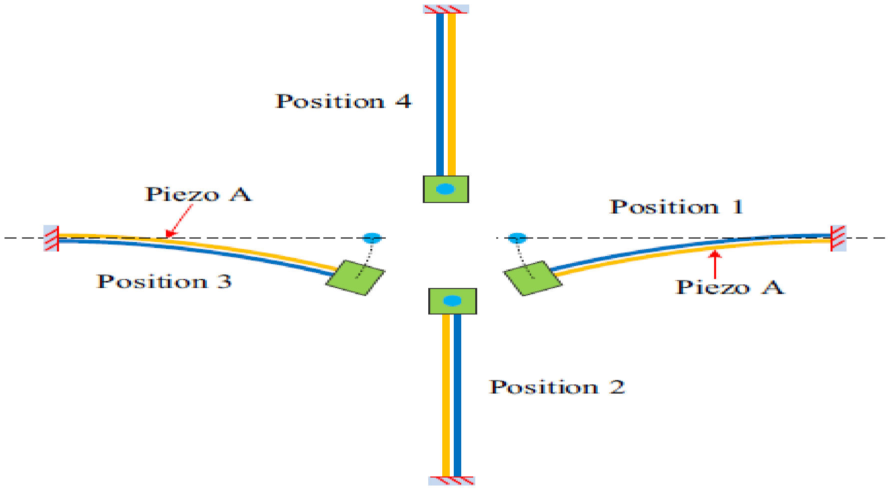

Figure 9: Typical beam configuration used by researchers [7]

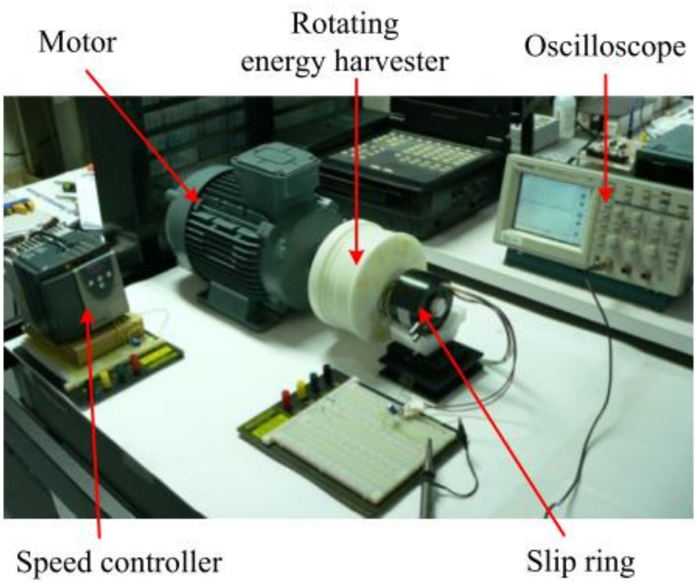

Figure 10: Experimental setup [7]

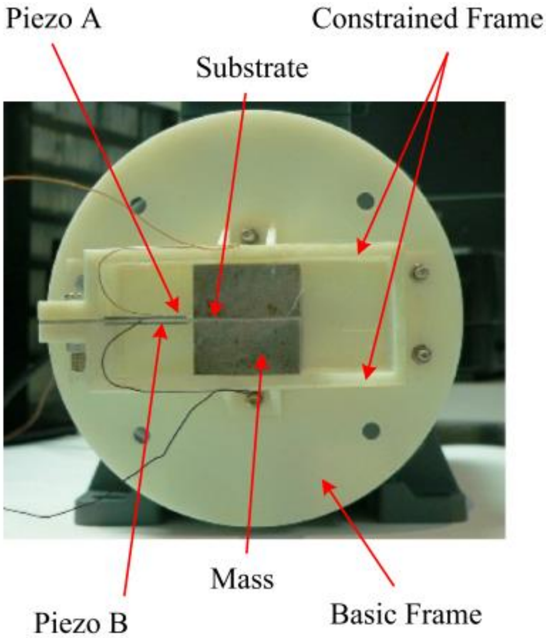

Figure 11: The harvester inside the AC motor [7]

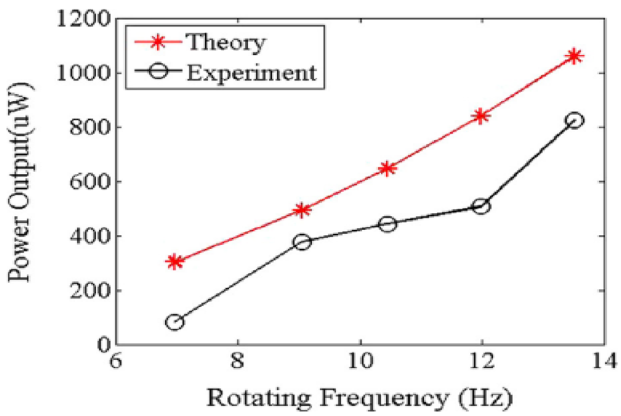

Figure 12: Simulation and experimental results [7]

Other researchers preferred to derive and solve the governing equation numerically with MATLAB® to analyze this configuration. Raja et al. [8] presented a similar design to the one in Figure 9, but the length of the beam was increased, the governing ordinary differential equation was derived using Euler-Bernoulli's beam theorem and solved the equation analytically. The FEM was used to numerically solve and validate the analytical solution of the equation and then get the voltage of the system. The results are verified experimentally. For the experimental setup the harvester on a desk which is attached to a shaft connected to an electric motor as shown in Figure 13. All results followed the same pattern where the produced voltage is increasing with the rotation speed in Hz, however the FEM and the analytical method did not match in number with the experimental results. Looking to the results obtained, in terms of accuracy, the FEM competes with analytical approaches; in most papers, the FEM shows a considerable agreement with empirical validations even in three-dimensional models. Additionally, impact configurations appear to harvest more energy than regular cantilever beams because the impact causes the material to deform more; however, the deformation may be extremely dangerous, and protective frames are required to prevent this. Table 1 summarizes the research done on softening beam effect configuration for piezoelectric energy harvesters.

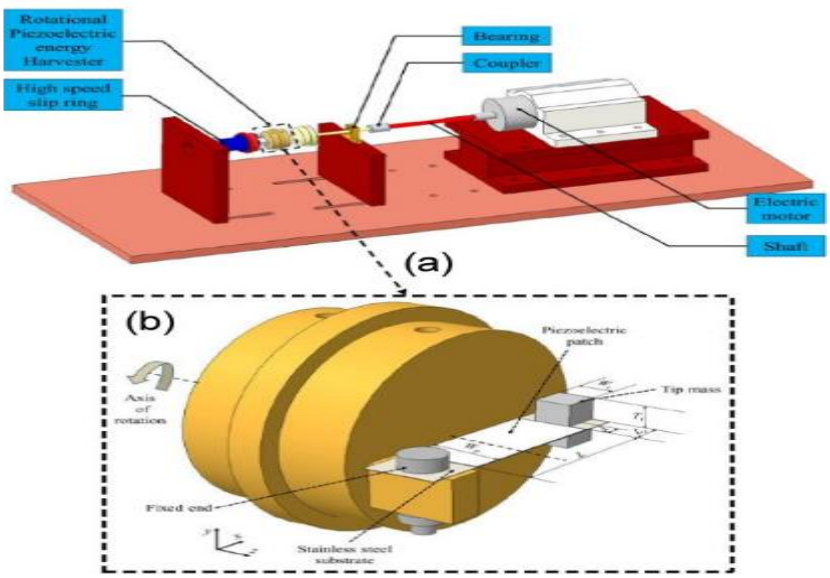

Figure 13: Experimental setup [8]

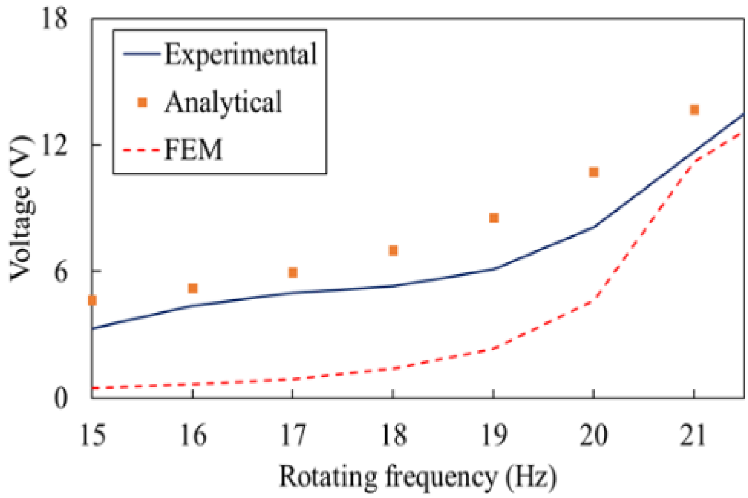

Figure 14: Simulation and experimental and analytical results [8]

Table 1: Summary of research done on softening effect

Structure type	Impact availability	Piezoelectric material	Rotating environment	Employed Technique	Results	Refs
Cantilever beam with a tip mass	No impact	PZT	General	Analytical solution	Power outputs:83.5 µW to 825 µW	[7]
Cantilever beam with a tip mas inside a limiting frame	No impact	Macro Fiver Composite	Tire rim	MATLAB® ODE solvers	82–1003 µW	[9]
Cantilever beam with a tip mass	No impact	PZT-5A	Slip ring	FEM	Peak power at 43.77 µW	[8]
Multi-cantilever beam with tip masses	Impact available	Macro Fiver Composite	General	MATLAB® ODE solvers	52.1µW at a rotation speed of 4.2 Hz	[6]
Cantilever beam with a tip mass	No impact	PVDF	Tire circumference	MATLAB® ODE solvers	The maximum voltage of 0.25 V	[10]
Cantilever beam with no tip mass	Impact available	PVDF	Rotating turbine case	MATLAB® ODE solvers	Maximum power of 2566.4 µW	[5]
Cantilever beam with a tip mass inside a frame	No impact	Macro Fiver Composite	General	MATLAB® ODE solvers	The maximum voltage of 16.33V	[11]
Cantilever beam with a tip mass	No impact	Macro Fiver Composite	General	MATLAB® ODE solvers	Maximum root mean square voltage 100 V	[12]

2.2.2 Stiffening Effect Inertial Excitation

The stiffening effect occurs when a cantilever beam fixed support is placed towards the center of rotation, some research papers have applied impact vibration on their systems and some implanted a cantilever beam in different rotational environments. However, Guo et al. [13] proposed a laminated piezoelectric plate in a rotary engine, the author developed an analytical model to predict the induced power from the harvester, the results are validated against the numerical solution done by the FEM, targeting the first two modes of vibration to obtain the induced electrical power. The results produced by the analytical model showed a great agreement, this shows the reliability of the model. Fang et al. [14] proposed a piezoelectric energy harvester with softening effect, where two piezoelectric beams were installed with their fixed end facing the center of rotation (stiffening configuration) with one impacting beam installed in the softening configuration as shown in Figure 15. The author conducted numerical simulation and experimental validation on three different impacting gaps, which are 1.07 mm, 1.43 mm, and 2.14 mm, and the results show an increase of the produced power by 212.5%, 258.7%, and 682.8% over energy harvesting without impact for each impacting gap respectively. They also, developed an analytical model for the similar structure with an impact gap of 0.75 mm. The results where compared against other literature, the maximum power showed an increase of 135.5% over energy harvesting without impact [15]. GU et al. [16] developed a stiffening piezoelectric cantilever beam with another cantilever beam which contains a tip mass that impacts the piezoelectric beam rabidly during rotation as shown in Figure 16. The resonant frequency of the harvester, an analytical model is proposed by the author to predict the resonance frequency under different forces and validate the results experimentally. The experimental composed of a fan that represent the rotating environment and the harvester its self-mounted on the center of the fan and a sensor to measure the deflection of the beam and another sensor to measure the voltage as shown in Figure 17. The experimental and the simulated resonance frequency are shown in Figure 18, the produced power with tuning resonance frequency is far greater than the power produced when the resonance frequency does not change Figure 19 show the power output comparison between the tuned resonance frequency without tuning resonance frequency. Regarding the non-impact beam configurations, all researchers used a cantilever beam placed in a rotating environment; however, the methodology used to assess the governing model differed from researcher to researcher; for example, one researcher used the finite element approach. Gedeon et al. [17] created a finite element model with a coupling formulation to compute the natural frequencies of the system using the quadrilateral element. For the experimental verification the Piezoelectric beam is mounted on a rotating shaft derived by a brushless DC motor of a top speed of 100 revolutions per minute, the other side of the shaft is mounted on a bearing as shown in Figure 20. The simulation findings are consistent with the experimental results (please see Figure 21).

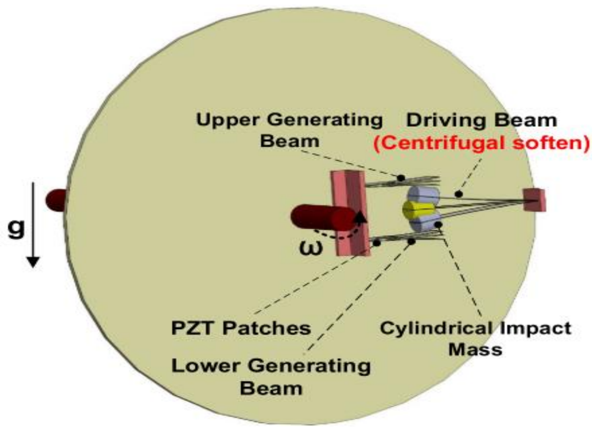

Figure 15: The schematic of the harvester [14]

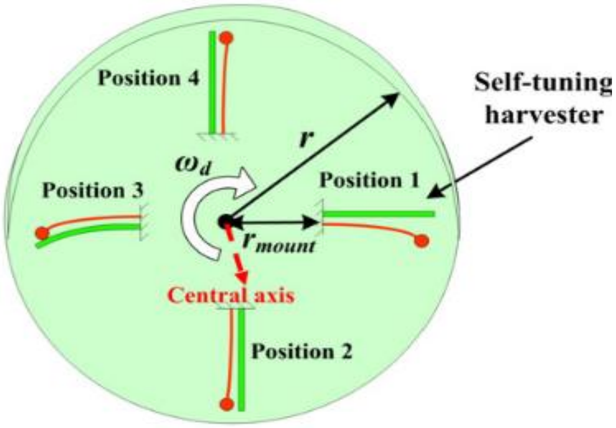

Figure 16: The harvester schematic [16]

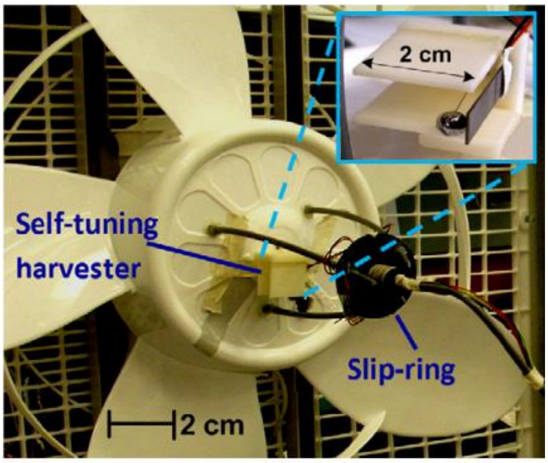

Figure 17: Experimental setup [16]

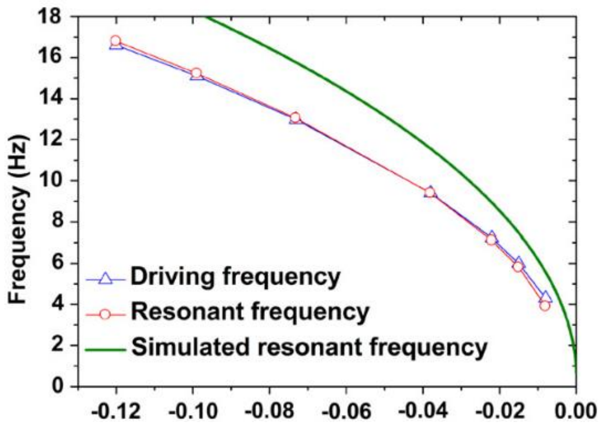

Figure 18: Simulated resonance and experimental resonance [16]

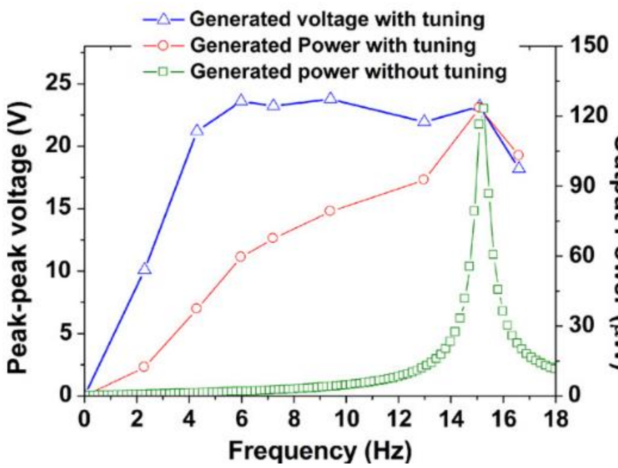

Figure 19: Power output comparison between the tuning resonance power and non-resonant power [16]

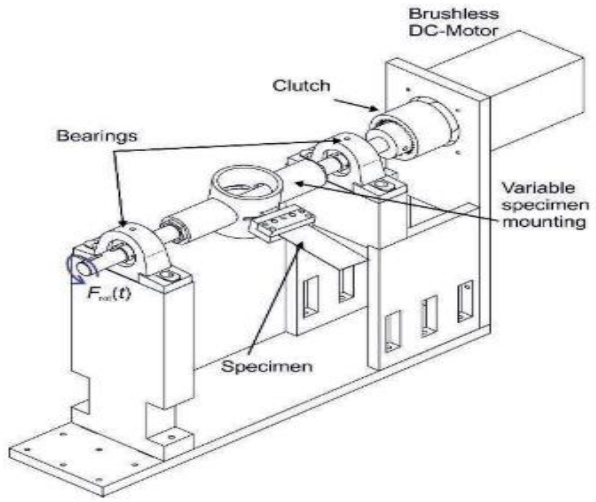

Figure 20: Experimental setup [17]

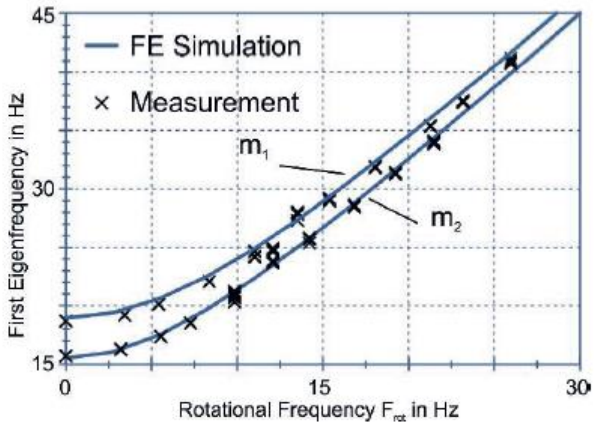

Figure 21: Simulation results along with the experimental results [17]

Hsu et al. [18] proposed a calculation procedure based on the FEM using the tetrahedral element. The result was validated against an analytical solution of the same system from the literature. The author further validated the result experimentally, regarding the experimental setup the harvester was attached to flexure mechanism. The flexure mechanism was attached to slip ring which was attached to a shaft, the weight was balanced using a balancing mass as shown in Figure 22. The resonance frequency measured by the three techniques is shown in Figure 23 and the induced power obtained in Figure 24.

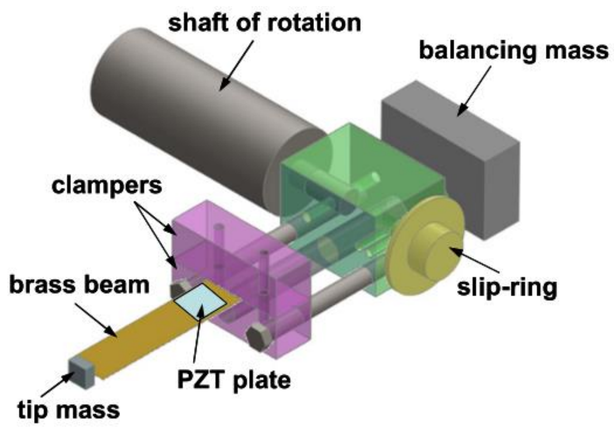

Figure 22: The experimental setup [18]

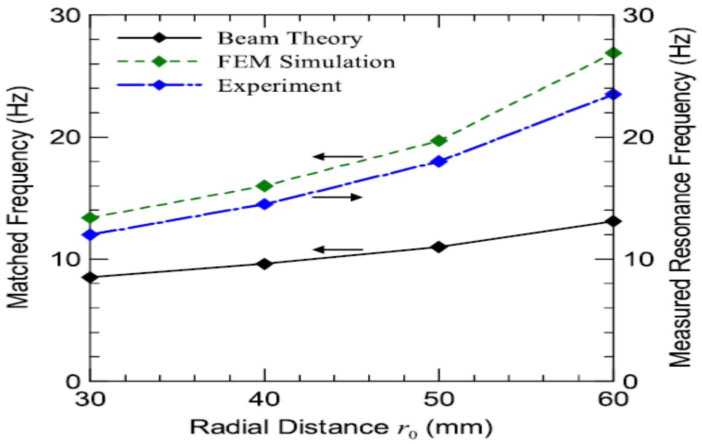

Figure 23: Resonance frequency calculation comparison [18]

Also in the stiffening effect, the finite element was showing a remarkable agreement with experimental or analytical solutions. Impacting configurations surpass the regular cantilever in terms of induced electricity but the cost might be very high deformation during vibration, protective frames are required to overcome this issue.

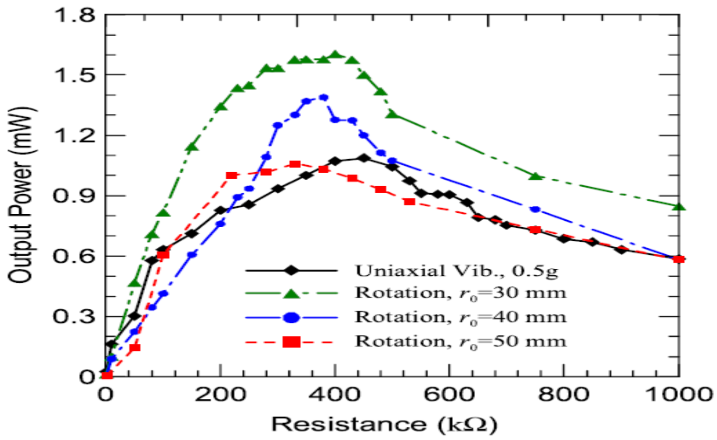

Figure 24: Power output from different vibrational configurations [18]

The majority used MATLAB® software to numerically solve the resulting governing equation using MATLAB®'s ordinary differential equation solvers. Different methods, such as the Lagrange formulation and the Hamilton principle, were used to derive the governing equation. Some researchers applied analytical formulation which showed a good accuracy with literature or experimental results, however, analytical solution does not suit every case since the formulation process is difficult and time consuming. Some of the researchers compared their simulation with finite element solution of their problems which shows the reliability of finite element method. All researchers applied PZT and its other types as the main energy resource, which showed high electrical capability comparing to other piezoelectric materials. The research publications that used the stiffening effect structural configuration are summarized in Table 2 .

Table 2: Summary of research done on stiffening effect

Structural type	Impact availability	Piezoelectric material	Employed technique	Results	Refs.
Multiple cantilever beams with tip masses	No impact	PZT	MATLAB®'s ODE solver	Maximum power output 20 mW at 29 Hz	[19]
Multiple cantilever beams with tip masses	No impact	PVDF and PZT	MATLAB®'s ODE solver	Maximum power of 6.4mW at a rotation frequency of 138 rad/s	[20]
Piezoelectric laminated plate	No impact	PZT	Analytical	Maximum power of 36.09 mW with an optimum resistive load of 11.4 kΩ a power of 293.58 mW with 16.6 kΩ	[13]
Multiple cantilever beam	No impact	PZT	MATLAB®'s ODE solver	The voltage output of 5 V at rotation frequency 65 Hz	[21]
Cantilever beam next to an impacting beam	Impact available	PZT	MATLAB®'s ODE solver	The power density of 30.8 µW cm^{-3}	[16]
Parallel piezoelectric beams with impacting beam	Impact available	PZT-5H	MATLAB®'s ODE solver	Root mean square voltage of 120V at a rotation frequency of 10 Hz	[15]
Trapezoidal beam with a tip mass	No impact	PZT-5H	MATLAB®'s ODE solver	The maximum output power of 0.42 to 0.74 mW at the frequency range of 8 to 28 Hz	[22]
Piezoelectric cantilever beam with a tip mass	No impact	Macro Fiver Composite	MATLAB®'s ODE solver	Maximum power of 0.61-6.28 mW at rotation frequency 7494.81 to 2498.27 Hz	[23]
Piezoelectric cantilever beam with a tip mass	No impact	Unspecified	MATLAB®'s ODE solver	Maximum power of 185 mW at rotation frequency 16.6 Hz	[24]
Parallel piezoelectric beams with impacting beam	Impact available	PZT-5H	MATLAB®'s ODE solver	The maximum power output of 0.5 µW at a rotation frequency of 9 Hz	[14]
Piezoelectric cantilever beam with a tip mass	No impact	PZT	MATLAB®'s ODE solver	Maximum power of 0.70 mW at a rotational frequency of 13 Hz	[25]
Piezoelectric cantilever beam with a tip mass	No impact	PVDF	MATLAB®'s ODE solver	Maximum power 65-110 µW at a rotation frequency 4 – 20 Hz	[26]

2.2.3 Axial Beam Configuration

For this configuration, the beam is parallel to the axis of rotation regardless of the fixed end direction of the beam, most of the research papers used multiple beams including the piezoelectric beam and a supporting beam connected with springs, for instance, Machado et al. [27] published a research paper for such configuration with slide changes. In the first paper, propose low excitation frequency with an impacting mass, numerical simulation is conducted to analyze the vibration-induced. The system has two springs, one connects the beams and one connects the impacting beam to the frame as shown in Figure 25.

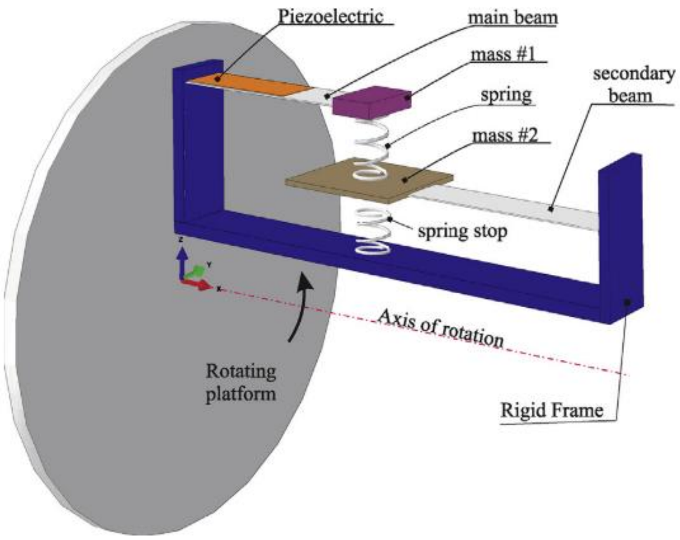

Figure 25: The proposed harvester adapted form [27]

The second paper introduced an analytical model to the same structure shown in Figure 25 but the spring which connects the frame with the second beam is removed to the end of the frame. The analytical model is verified via numerical simulation and experimentation [28]. Febboa et al. [29] with the help of the previous author produced the third paper experimenting with the structure shown in Figure 25 and validating the results with analytical solutions from literature, the curve fitting of the analytical solutions with the experimental results are shown in Figure 26. For experimental setup was similar to Figure 25 but the whole structure was attached to an induction motor to represent the rotary motion. The energy harvested from the first paper produced higher power than the one without the spring connecting the frame to the second beam. It can be seen that springs might increase the deformation of the beam and thus increasing the energy induced by the system.

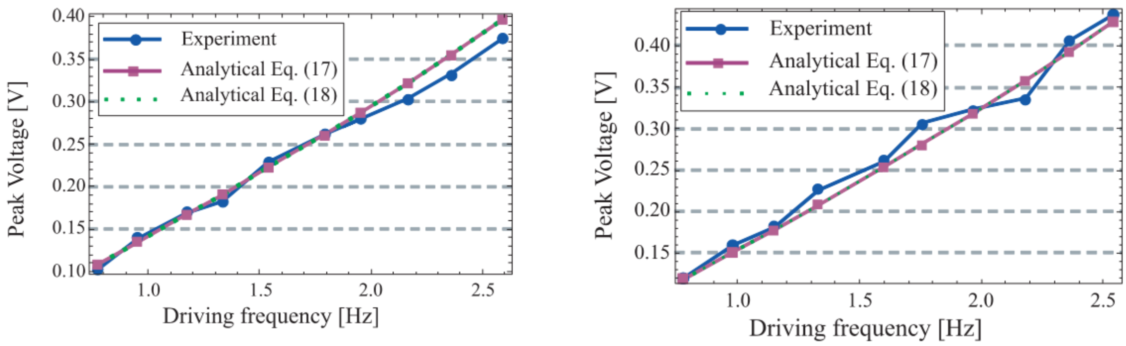

Figure 26: Experimental results compared with the analytical solution, the left graph is when the beam doesn't have a mass and on the right graph the beam is having an extra mass [29]

Some research papers used only one cantilever beam for the axial configuration, for example. Leinonen et al. [30] developed a finite element model to analyze the beam which was a tapered beam composed of two piezoelectric layers on top and bottom with one substrate in the middle, the beam is shown in Figure 27. The results show that the maximum power was 6 mW at 3600 RPM, for experimental part the experimental setup was composed of the piezoelectric beam attached to a desk which was connected to a DC motor, a data logger was installed on the desk also to capture the voltage produced from the harvester as shown in Figure 28. However, the majority of the research papers preferred to apply multiple beams to simulate these systems, again the FEM proved useful in analyzing piezoelectric energy harvestings systems where accuracy was highly competitive against analytical solution and Runge-Kutta method used in MATLAB, still Euler-Bernoulli model to model the behavior of the piezoelectric beams with FEM approach Table 3 contains the summary of the search papers that applied axial beam configuration.

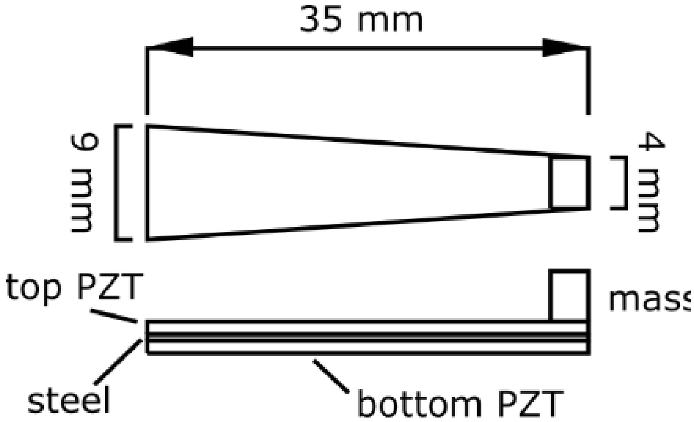

Figure 27: The schematic of the beam [30]

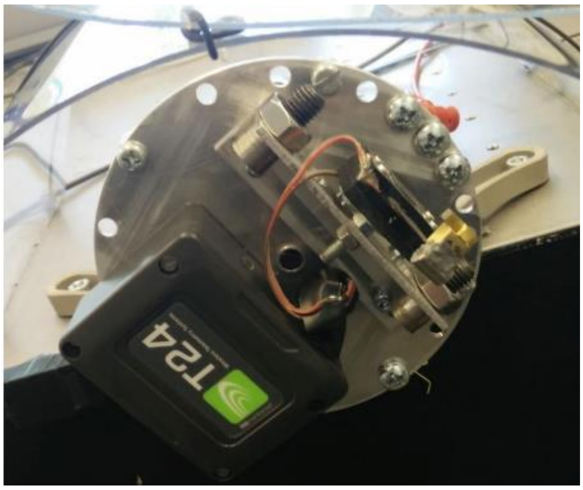

Figure 28: Experimental setup [30]

Table 3: Summary of research done on axial configuration

Structural type	Impact availability	Piezoelectric material	Employed technique	Results	Refs.
Multi-beam	No impact	PZT	FEM	Maximum power of 1.14 mW on rotation frequency of 4.36 Hz	[31]
Multi-beam	No impact	Macro Fiver Composite 2814 P2	FEM	Maximum electrical power of 200 μW in the rotation speed of 0.5 to 3 Hz	[32]
Multi-beam	No impact	PZT	Experimental model	The peak voltage of 20 V with a rotational frequency of 17 Hz	[33]
Multi-beam	No impact	MIDE	FEM	The peak voltage of 0.20 V at a rotation frequency of 6 Hz	[34]
Multi-beam	Mo impact	PZT-5A	Analytical model	Induced electrical power of 26 to 105 μW at a rotation frequency of 0.83 to 2.50 Hz	[29]
Cantilever beam with tip mass	No impact	PZT-5A	FEM	Maximum electrical power of 15 μW at a rotation frequency of 7.5 Hz	[30]
Multi-beam	No impact	PZT-5A	Analytical modeling	Maximum power if 151.202 μW at a rotation frequency of 2.2 Hz	[35]
Multi-beam	No impact	PZT-5A	Analytical modeling	The output power of 125 μW at a rotation frequency of 0.7 to 2.5 Hz	[28]
Multi-beam	No impact	PZT-5A	MATLAB®'s ODE solvers	Maximum power between 102 to 845 μW at the rotation frequency range of 0.83 to 2.5 Hz	[27]

2.3 Magnetic Excitation

Magnets are used as additional excitation elements besides gravitational excitation to optimize the peak displacement due to vibration, magnets have proven that it can significantly increase the harvested power. The common configuration that researchers use when they wish to use magnets is a magnetic poof mass placed at the free end of the cantilever beam and frame which contains another magnet exactly in front of the beam to generate the magnetic excitation force as a magnet. For instance, Mei et al. [36]. who proposed the configuration shown in Figure 29a and inserted it inside a tire rim, here beside the gravitational excitation and magnetic excitation there is the random excitation which is caused by the roughness of the road as shown in Figure 29b. This vibrational noise is rather beneficial then unwanted because there is one phenomenon which can be used to employ the noise to the advantage and maximize the deflection due to the vibration, this phenomenon is called stochastic resonance. For this phenomenon to happen the system has to be bi-stable or in other words having more than one stable position and also the deterministic vibration should be equal to the stochastic frequency. The governing equation derived by the author includes the noise excitation, and then the equation is solved using MATLAB® ordinary differential equation solvers. The experimental setup used by the other was composed of the energy harvester mounted on a plate which is attached to a motor, the motor is controlled by a computer via motor driver, an oscilloscope to monitor the voltage produced form the harvester. A laser sensor was also mounted to measure the deflection of the harvester during vibration, the experimental setup is shown in Figure 30. The experimental results showed a great agreement with the simulation result as shown in Figure 31 and Figure 32 and Figure 33.

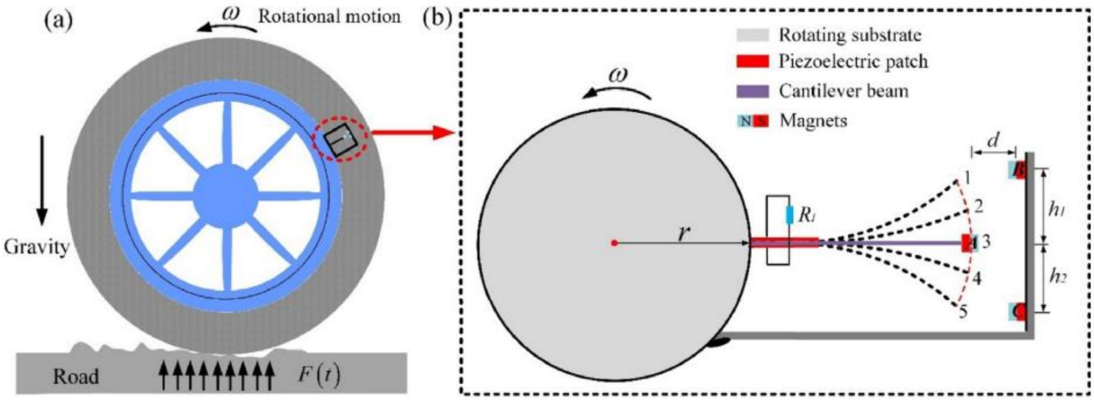

Figure 29: Common configuration used by researchers [38]

In Figure 31 and Figure 32 and Figure 33, the peak voltage is always 2V for every rotational frequency [36], Zhang et al. [37]. Also proposed a similar structure to the one shown in Figure 29 and under the same rotational environment and the same condition but a stiffening configuration was employed. The outputted voltage was 7.3 V across a 150 kΩ at a frequency band of 31 rad/s to 129.4 rad/s, this result is higher than softening configuration by the previous author, However, softening configuration related researches were far less than the stiffening configuration ones.

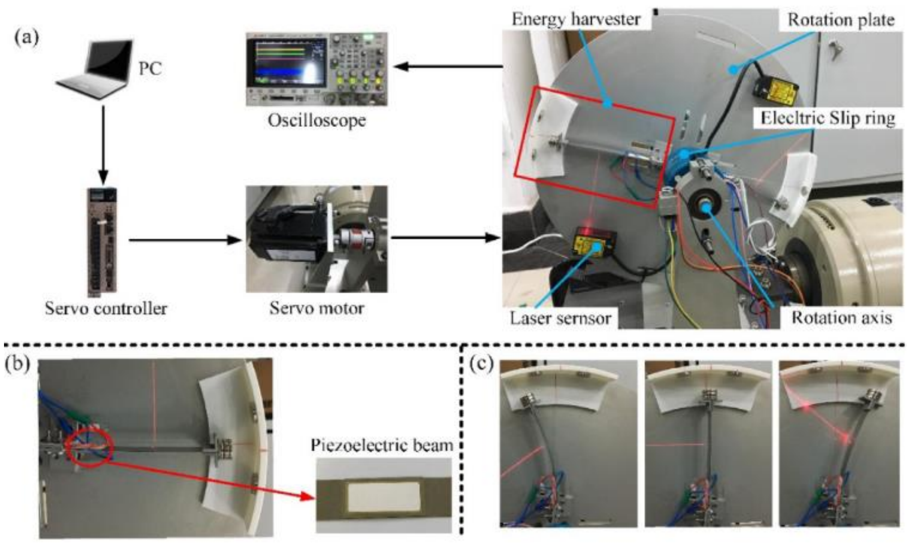

Figure 30: Experimental setup [36]

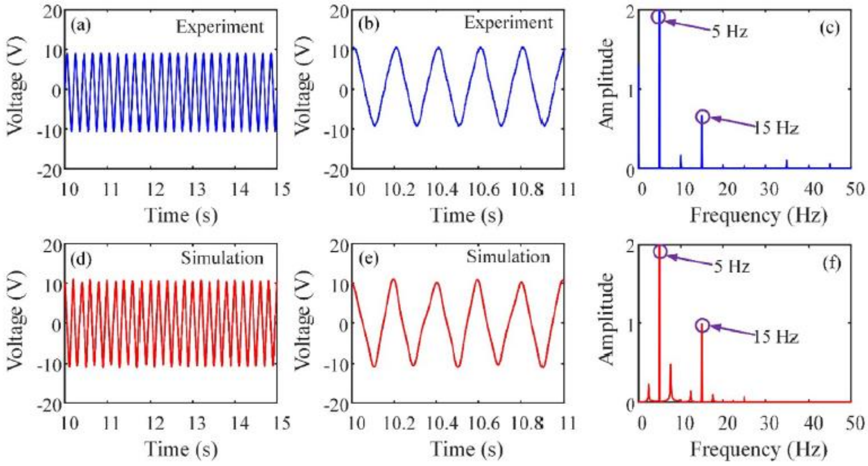

Figure 31: Voltage output at a rotational frequency of 300 rpm or 5 Hz [36]

Some researchers did apply impact to their structure, for instance, Fang et al. [38]. Proposed softening effect beam configuration, the structure consists of an impacting beam and two piezoelectric patches installed in a rotating body with a magnetic poof mass and another magnet is at the center of rotation. The system is also experiencing random excitation due to the impact thus the stochastic resonance technique was employed in this system.

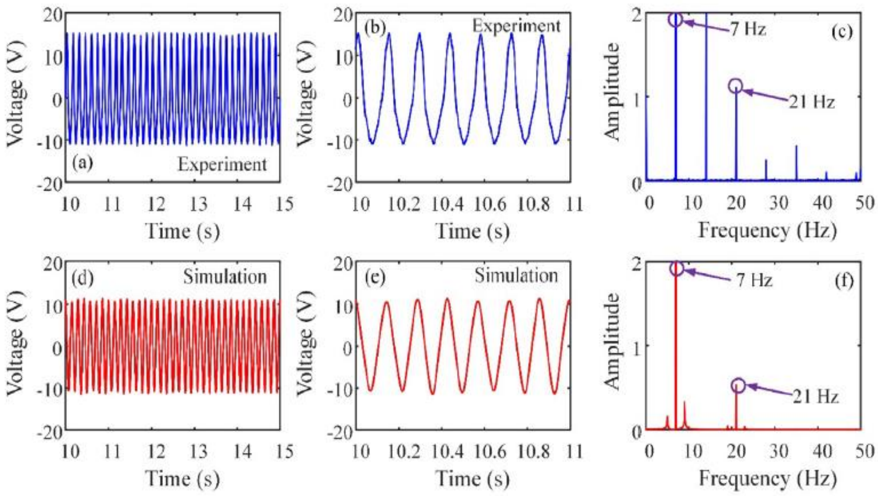

Figure 32: Voltage output at a rotational frequency of 420 rpm or 7Hz [36]

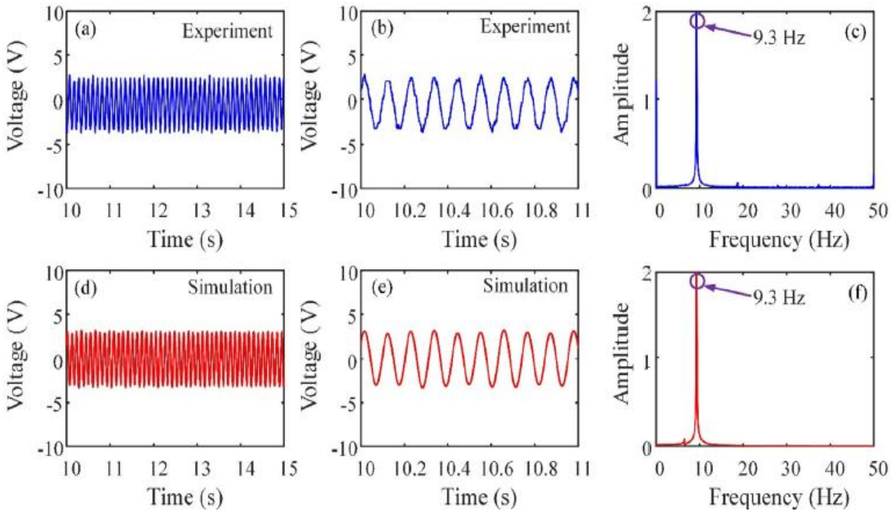

Figure 33: Voltage output at a rotation frequency of 560 rpm or 9.3 Hz [36]

However not all research took random excitation into account such as Zou et al. [39] who proposed a multi-beam structure, the structure consist of two cantilever beams with magnet tip mass hanged on each beam, each beam is in softening configuration as shown in Figure 34. The derived governing equation was solved using MATLAB® ordinary differential solvers the results are verified with experimentation. The experimental setup was composed of a servo motor which rotates to energy harvester and a signal acquisition to capture the produced voltage and a computer to process the data as shown in Figure 35a. In Figure 35b two prototypes were mounted in the setup one with only one beam and the other with two beams, the experimental results were in great agreement with the simulation results as shown in Figure 36 where the curve fitting shows a very small error for both prototype A and prototype B. However at around 450 RPM there a small error in the peak produced voltage between the experimental prediction and the conducted simulation. Also, Mei et al. [40] developed a cantilever beam structure inside a blade of a wind turbine, the cantilever beam was attached to a magnetic tip mass with two masses attached in front of it as shown in Figure 37. The theoretical model is established, and validated with experimental procedures, the experimental setup composed of rotating desk with the energy harvester mounted on it, the harvester is connected to data acquisition system to capture the voltage, Figure 38a shows an outward configuration and Figure 38b shows the inward configuration. The results showed that the softening effect outcomes the stiffening effect in the produced voltage where as shown in Figure 39 both the experimental and simulation results of the softening effect exceed the results from the stunning effect which indicates that the buckling behavior produced higher voltage then tensile behavior, Table 4 is summarizing the research paper with magnetic excitation.

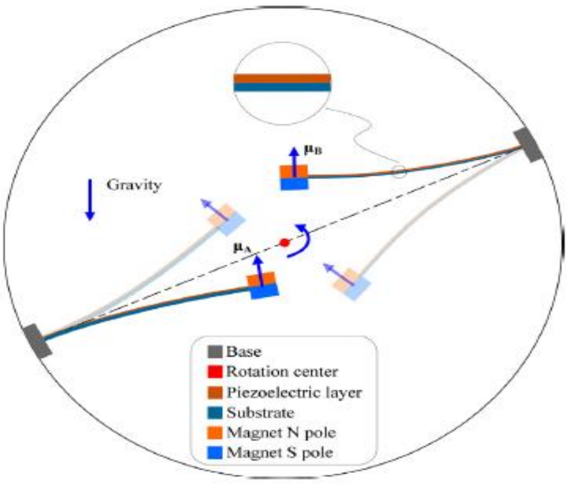

Figure 34: Multi-beam configuration [39]

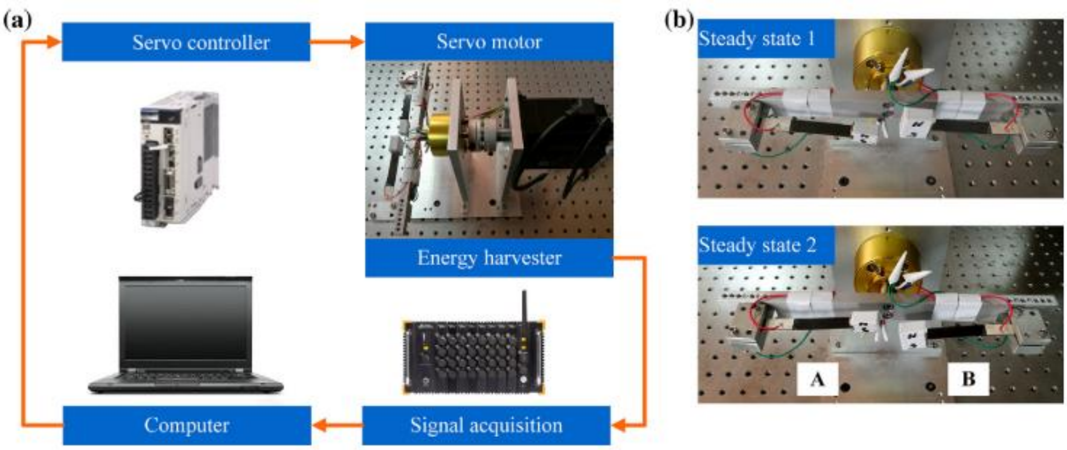

Figure 35: The experimental setup [39]

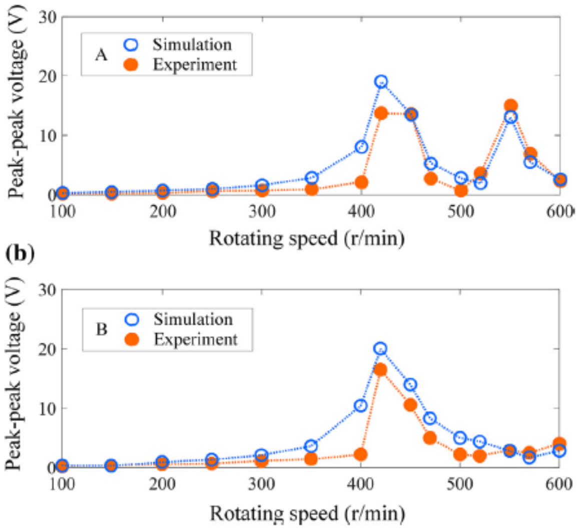

Figure 36: Experimental results with simulation results, A is the rotating speed at 7 Hz and B is the rotating frequency 9.17 Hz [39]

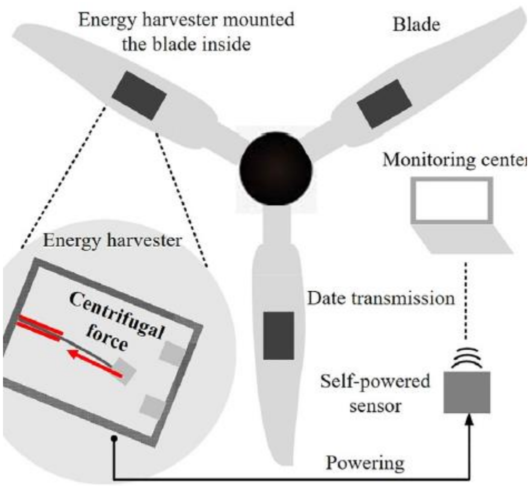

Figure 37: The schematic of the system[40]

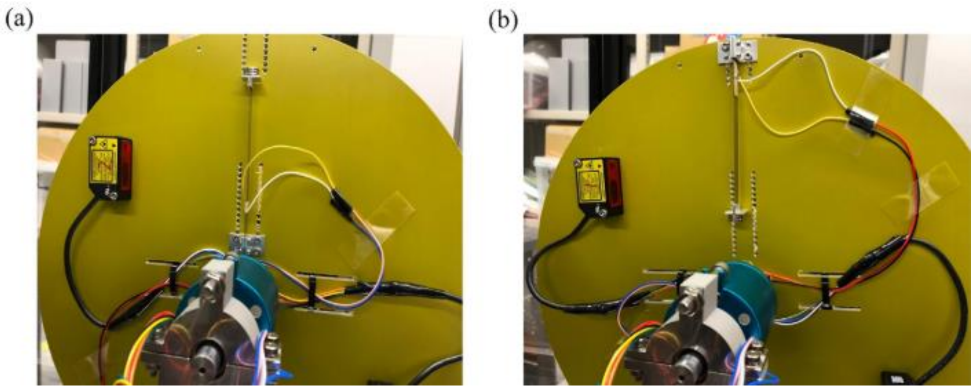

Figure 38: Experimental setup a is the outward beam configuration and b is the inward beam configuration [40]

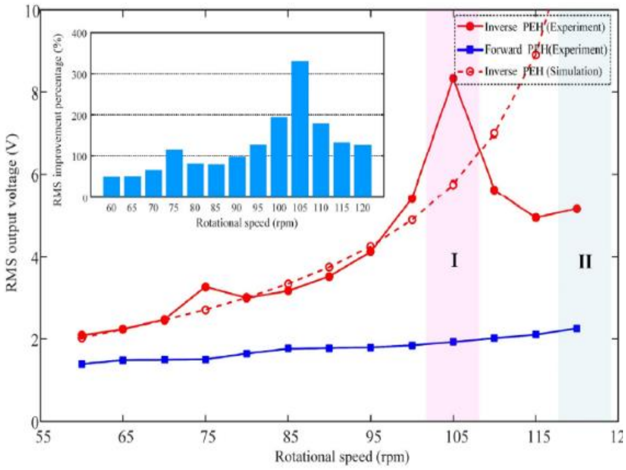

Figure 39: Simulation results and experimental results[40]

Table 4: Summary of research on magnetic excitation

Structural type	Impact availability	Piezoelectric material	Employed technique	Results	Refs.
Softening configuration	Impact available	PZT	MATLAB® ODE solver	Peak power: 2.50 mW, Rotation frequency 5.30 Hz	[36]
Softening configuration	No impact	PZT	MATLAB® ODE solver	The Peak power: 0.21 mW	[37]
Softening configuration	No impact	PZT	MATLAB® ODE solver	Peak power: 564 µW, at rotation frequency: 7 Hz , Peak power: 535.3 µW , at rotation frequency: 9.17 Hz	[38]
Softening configuration	No impact	PZT	MATLAB® ODE solver	The power density of 0.76 µW / cm^{-3}	[41]
Softening configuration	No impact	PZT	MATLAB® ODE solver	Peak voltage: 5 V, Rotation frequency: 2.7 Hz	[39]
Softening configuration	No impact	PZT	Analytical modeling	Peak voltage: 4 V, Rotation frequency: 2 Hz	[42]
Stiffening configuration	No impact	PZT	Analytical modeling	Peak voltage: 7 V, rotation frequency: 8 Hz	[43]
Stiffening configuration	No impact	PZT	MATLAB® ODE solver	Peak voltage: 2 V, Rotation frequency: 5 Hz, Rotation frequency: 7 Hz Rotation	[40]

				frequency of 9.3 Hz	
Stiffening configuration	No impact	PZT	FEM	Peak power: 15.425 mW, Rotation frequency of 2.5 Hz	[40]
Stiffening configuration	No impact	PZT	Analytical modeling	Peak voltage: 7V, Rotation frequency 50 Hz, Peak voltage: 4.3 V, Rotation frequency: 250 Hz	[36]
Stiffening configuration	No impact	PZT	MATLAB® ODE solver	Peak power: 0.14 mW, Rotation frequency: 15.59 Hz	[44]
Stiffening configuration	No impact	PZT	MATLAB® ODE solver	Peak power:4 mW Rotation frequency: 12 Hz	[45]
Softening configuration	No Impact	PZT	MATLAB® ODE solver	Peak power: 80 µW Rotation frequency: 2 Hz	[46]
Softening configuration	No impact	PZT	Analytical model	Root mean square voltage:0.25 V	[47]
Stiffening configuration	No impact	PZT	MATLAB® ODE solver	Peak voltage:5 V, Rotation frequency: 7.5 Hz	[48]
Softening configuration	No impact	PZT	MATLAB® ODE solver	Peak power: 50 µW Driving speed: 25 km/h	[49]
Softening configuration	No impact	PZT	Analytical modeling	The peak voltage was 0.65	[50]
Softening configuration	No impact	PZT	Analytical modeling	The Peak power: 500 µW, Rotation frequency:5.83 Hz	[51]

2.4 Summary of the Chapter

In this chapter, a comprehensive review is presented of the recent techniques and development of piezoelectric energy harvesting in rotating environments. The structural designs and the employed techniques of simulation are discussed and compared. It is been concluded that the FEM was not employed enough in the literature where the majority used MATLAB® ode solver and developed analytical methods to analyze the structure at hand. Light materials was not employed in the structures where the substrate was a random metal. Regarding the structural configuration, the impacting structural configuration indeed achieved high power output from the harvesters at hand which suppresses the configurations which did not employ impacting in most cases, however there is a big disadvantage which is the probability of destruction of the harvester due to very high deformation caused by the strong impact. Protective cases are provided to prevent this issue, another solution was to model a multi-beam configuration where a beam is responsible to impact the beam which contain the piezoelectric layer, but the chance of over deformation is higher. Some non-impacting configuration produced a competitive power to the impacting configuration due to the high rotation frequency of the environment, but there is a threshold to the rotation frequency were very high rotation frequencies prevent the harvester from deformation enough to produce energy. Another solution was to add more beams into the same rotation environment to add-up the produced power, however some cases who used different material for substrate which produced higher power than others. Though thermal investigation was not present on the researchers where nearly no one applied temperature on the harvester to observe the energy behavior since temperature might vary in industrial environments and machineries.

Chapter 3

RESEARCH METHODOLOGY

In this chapter the research methodology followed by this thesis is going to be presented. This chapter will be divided into four sections the first section is the modal proposed and the second section is the finite element preprocessing of the problem. The third section is noise inheritance to the results of the finite element simulation of the electrical potential to boost it even further. The fourth section is investigating the temperature effect on the output power of the proposed energy harvester, the research methodology flowchart is illustrated in Figure 40.

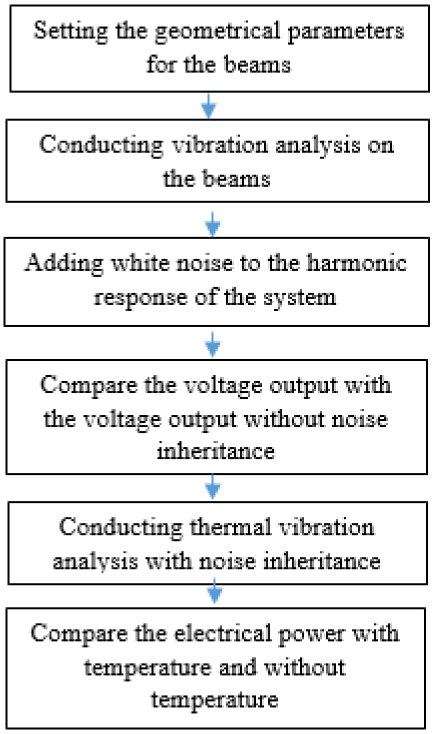

Figure 40: Research methodology flow chart

3.1 Proposed Beam Model

The beam model was adapted from the thesis by Gustav et al. [52] which was a cantilever sandwich beam consisting of a piezoelectric layer and two substrate metals on the bottom and two tip masses at the free end of the beam. This configuration is chosen becnause is meets the objectives of this study, since the beam has two metallic substrates that support the beam and prevent it from overdefoming, however deformation is needed to make the piezoelectric layer produce electrical energy. Substrats partially effect the power output since metallic substrats have the ability to conduct electrical energy and thermal energy, thus optimizing the maximum defomration and the maximum electrical output. The geometrical details are presented in Table 5, the simulation was done on COMSOL software and the resonance frequency obtained was 67 Hz, the resonance frequency was validated on ABAQUS® software. The noise was added to the frequency response using MATLAB® software to validate the output power of 370 μW across an optimal resistance of 70 kΩ to produce such power. The voltage from the PZT-5J should be around 5 V. The resonance frequency obtained from the simulation is 67.20 Hz which is a 0.20 Hz difference from Gustav et al. [52].

Table 5: Geometrical parameters of the proposed beam from [55]

Layer	Dimension (L × W × t)
PZT-5H	$58 \times 6.80 \times 0.25\ mm^3$
Substrates 1&2	$58 \times 6.80 \times 0.70\ mm^3$
Proof mass	$6.80 \times 4.0 \times 4.0\ mm^3$

The power obtained from noise addition was 360.9 μW which is 0.1μW. The proposed modal is adapted from Gustav et al, the piezoelectric material in the thesis was PZT-

5J wherein the proposed structure is PZT-5H. Regarding the subtract material, three beams models will be created each with a different material in the substrate with the same piezoelectric material. Frequency response analysis will be done and white noise will be added to the frequency response for each beam and it will be compared with each other. The results will be compared with the Gustav et al, the geometrical parameters used in this thesis is no difference from Gustav et al. Table 5 contain the geometrical details for each beam. Table 6 shows the material properties applied on the substrate and. Table 7 showed PZT-5H electrical and mechanical material properties since the material is not isotropic the properties will differ depending on the plane of the PZT-5H.

Table 6: Simulation parameters for substrates and tip mass on the proposed model

Model	Material	Density Kg/m^3	Young's modulus (Pa)	Poisson's ratio (Unit less)
Beam model 1	Aluminum	2500	68000000000	0.3
Beam model 2	Magnesium	1738	45500000000	0.295
Beam model 3	Titanium	4500	220000000	0.34

The tip mass material properties will the same as the substrate material properties for each model to optimize the beam durability and the amount of deflection occurring to the beam. If the material of the substrate and the tip masses are the same then the tip mass will apply the maximum load due to the material and the substrate material will offer maximum load resistance due to the material. The fact that the substrate and the tip mass have the same material this will insure that no one will deform the other during vibration.

Table 7: PZT-5H properties

PZT-5H		
Density	7500	kg/m^3
D11	1.51E-08	F/m
D22	1.55E-08	F/m
D33	1.30E-08	F/m
E1	6.06E+10	Pa
E2	6.06E+10	Pa
E3	4.83E+10	Pa
Nu12	0.289	Unit less
Nu13	0.512	Unit less
Nu23	0.512	Unit less
G12	2.35E+10	Pa
G13	2.3E+10	Pa
G23	2.3E+10	Pa
d113	7.41E-10	m/V
d223	7.41E-10	m/V
d311	-2.74E-10	m/V
d322	-2.74E-10	m/V
d333	5.93E-10	m/V

3.2 Finite Element Modeling in ABAQUS

The proposed beams will be in the same rotational environment conditions applied by Gustav et al hence there will be a centrifugal force acting on the beams making the displacement response following the Euler-Bernoulli beam theorem [57]. For the vibrational analysis the modal analysis and the steady-seat analysis will be performed.

3.2.1 Boundary Conditions

Since there is a piezoelectric material included in the structure there will be two types of boundary conditions, the first one is the mechanical boundary condition and the second one is the electrical boundary condition.

3.2.1.1 Mechanical Boundary Condition

The proposed beam modal is a cantilever beam that will be hung on the circumference of the rotation, hence the centrifugal force will compress the beam. Figure 41 shows the cantilever beam boundary condition for modal analysis. Figure 42 shows the concentrated force boundary condition which was the centrifugal force for steady-seat analysis which have a magnitude of the total mass of the beam times the central acceleration.

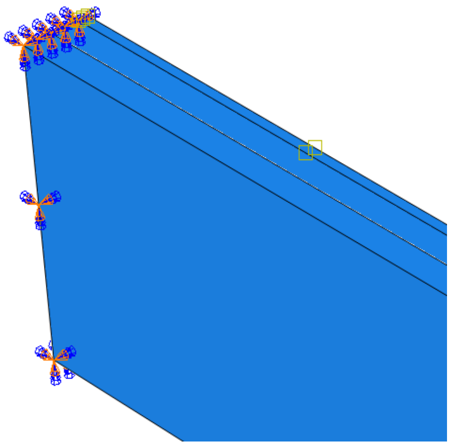

Figure 41: Fixed Support boundary condition

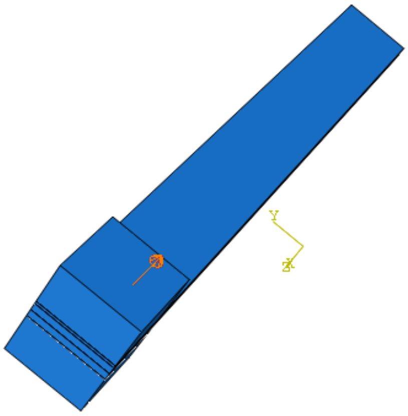

Figure 42: Centrifugal force boundary condition

3.2.1.2 Electrical Boundary Condition

The piezoelectric material will have electrical flow once it is deformed since, for electrical energy to flow a ground that has zero potential is needed so that the electrons will flow during deformation. Figure 43 showed the grounding on the bottom of the piezoelectric potential so that the voltage will appear on the top and the sides of the piezoelectric material.

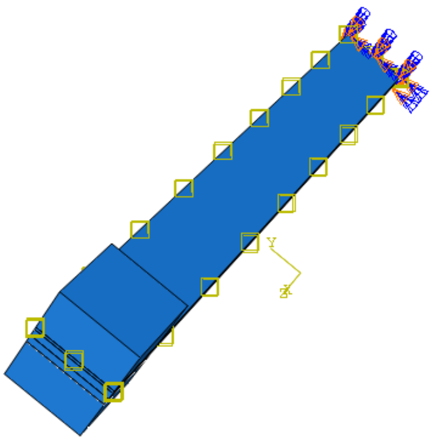

Figure 43: Grounding boundary condition for the piezoelectric material

3.2.2 Meshing

The meshing process is divided into two crucial parts, the first one is assigning the element type that will capture the degree of freedom of the beam and the second one is assigning the mesh control that will present the geometry of the beam properly.

3.2.2.1 Element Type

The beam is composed of three layers and two tip masses, two of the layers are substrate material and the third layer is piezoelectric. Regarding the two substrate layers and the tip mass, a 3-dimensional stress element is chosen to capture the rotation and translation of the x-axis and y-axis and z-axis wherein the piezoelectric layer piezoelectric element is chosen to capture the electrical degree of freedom on the piezoelectric material. Table 8 summarizes the element type chosen for each layer. Reduced integration technique was applied to simplify computation and reduced the required time to produce the results.

Table 8: Element type for each layer and the tip mass

Layer	Element Type	Name of Type
Piezoelectric Layer	C3D20RE	Piezoelectric element with reduced integration
Substrate Layer	C3D20R	3-D stress element with reduced integration
Tip Mass	C3D20R	3-D stress element with reduced integration

3.2.2.2 Mesh Control

The meshing shape must be able to present the geometry properly for each layer, since all layers are rectangular, the quadratic tetrahedral element will be the most suitable for each layer making the mesh for the whole beam. The piezoelectric layer had 2436 elements and the substrates had 239 elements each which makes 478 elements in total and the tip masses had 184 elements each which makes 368 elements in total. The total number of elements on the whole beam is 3282 elements, Figure 44 shows the meshed beam geometry for all layers.

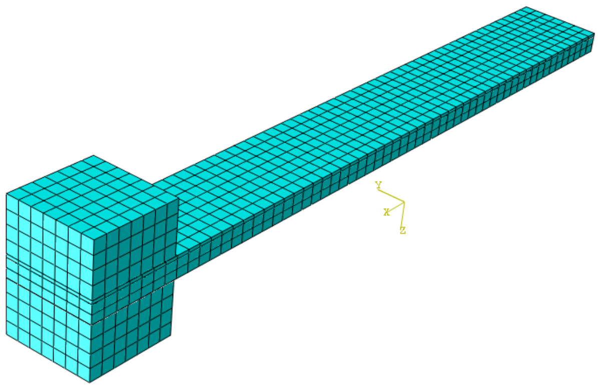

Figure 44: The meshed beam

3.3 Adding Noise to the Response of the System

The noise used in this thesis is Gaussian white noise which is a collection of random points in the time domain following Gaussian distribution which has a standard deviation of 1 and a mean of zero [53]. After the steady seat response of the beams is calculated the data is transferred to MATLAB®. In MATLAB® the steady-state responses are transferred from frequency domain to time domain using the “ifft” function which stands for inverse fast Fourier transform and then the Gaussian white noise will be applied using random function which is a random number generator. This function can generate a random number according to the need. Then the results is transferred back to the frequency domain using “fft” function which stands for fast Fourier transform. This process will be applied to each beam.

3.4 Temperature Effect

In this section the temprature effect will be investgated , the expremintal data along with there refarcnes are ullistrated in Table 9 Curve fitting schemes are curried out using "cftool" from curve fitting tool box in MATLAB® to obtain the material properties in the temperature range from 50°C to 150°C with 10°C in step size to carry out the finite element simulation to obtain the electric potential versus frequency graph on each temperature for each material to investigate the temperature influence on the produced voltage. Then the noise is going to be added and power output for each beam is going to be calculated and compared to the power output with no temperature effect.

Table 9: Experemintal data and there refrances

Experemintal data	Refs
Young modulus Vs temprature (Aluminum)	[54]
Young's modulus VS temprature (Magnesium)	[55]
Young's modulus VS temprature (Titanium)	[56]
Young's modulus VS temprature (PZT-5H)	[57]
Dielectric constent VS tempature (PZT-5H)	[57]
Electro-mechanical coupling factor VS temprature(PZT-5H)	[57]

3.5 Summary of the Chapter

In this chapter, the analysis input boundary conditions for both modal analysis and harmonic analysis are discussed. Also, the modal used in this thesis and the modal adapted from Gustav et al are discussed in terms of geometry and material selection. The validation of the results obtained by Gustav et al are carried out for the resonance frequency of the beam and the peak power after noise inheritance on the beam. The aim and preparation of the simulation study are discussed and demonstrated. Curve fitting schemes for the material properties under different temperatures to obtain the exact material properties for the desired temperature range are discussed.

Chapter 4

SIMULATION RESULTS

In this chapter, a comparative study is carried out between titanium, magnesium, and aluminum, all with PZT-5H piezoelectric material in terms of modal and steady-state analysis results with added noise. The modal and harmonic analysis are carried out again but in the different temperature ranges to see the effect of temperature.

4.1 Modal Analysis

Modal analysis is the process of obtaining the natural frequencies and mode shapes of the structure of interest and also extracting the effective mass in X and Y and Z directions in each mode to have the ability to predict which mode shape will be dominant if a certain force is applied in a certain direction and a certain frequency. Since the structures have natural frequencies, if the applied frequency is close to the natural frequency of a certain model then that mode is most likely to appear, however, other modes might appear if the excitation frequency is also closed to other natural frequencies of the other modes. In Aluminum and Titanium and Magnesium the result showed that the dominant mode shape is the fifth mode shape since it has the highest mass participation in the x-direction column as shown in Table 10 and Table 12. Except in Table 11 where the first mode shape is dominant because it has the maximum value in the x-column since the applied force is acting along the negative x-axis as shown in Figure 42. Which is also going to results in rotation about the y-axis and translation on the z-direction since the fifth mode row for aluminum and titanium and first mode row for magnesium has the highest mass participation. In the z translation direction and the highest mass participation as shown on Tables 10- 12 and in the y-rotation as shown in Tables 13- 15. The natural frequencies of and peak electrical potential of each mode for aluminum and titanium and magnesium are shown Tables 16-18.

Table 10: Aluminum and PZT-5H effective mass of translation coordinates

Mode Shape	x-Translation	y-Translation	z-Translation
1	3.02E-10	1.92E-12	0.0179759
2	4.78E-23	0.0180544	3.65E-12
3	2.44E-16	1.24E-08	9.51E-16
4	2.53E-08	4.02E-12	0.000510085
5	5.62E-07	7.16E-15	0.000249647
Total effective mass	5.88E-07	1.81E-02	1.87E-02

Table 11: Magnesium and PZT-5H effective mass of translational coordinates

Mode shape	x-Translation	y-Translation	z-Translation
1	4.76E-09	1.34E-12	0.00122548
2	9.39E-10	7.00E-09	2.34E-04
3	8.39E-15	1.23E-03	1.27E-09
4	2.85E-13	4.28E-08	9.65E-10
5	8.95E-10	2.83E-12	7.52E-05
Total effective mass	6.59E-09	1.23E-03	1.53E-03

Table 12: Titanium and PZT-5H effective mass of translational coordinates

Mode shape	x-Translation	y-Translation	z-Translation
1	1.10E-07	7.16E-12	0.0025002
2	1.33E-06	2.61E-09	3.51E-04
3	3.42E-10	2.61E-05	2.44E-08
4	5.53E-13	2.48E-03	5.27E-11
5	2.48E-06	3.91E-10	0.00011124
Total effective mass	3.92E-06	2.51E-03	2.96E-03

For aluminum in Table 10 , the fifth mode shape value has mass participation of 58.86% which is the maximum mass participation in the x-translation column in translational coordinates where the force is applied since the third, and fourth mode shapes have very weak mass participation compared to mode two and three and five there for their frequencies are neglected. Following the fifth mode row the highest effective mass is 8.55E-05 in the z-translation column, for rotational coordinates in the fifth mode shape row has the highest value of 6.71E-07 which is in y-rotation column there for the expected behavior is bending since most of the mass participated in mode shape 5 are translating through the z-axis and rotating around the y-axis. The electrical potential for the second mode shape is the second maximum after the fifth mode shape as shown in Table 16. For the titanium beam in Table 12. The max maximum effective mass participation on the translational x-axis is 63.27% so the third, and fourth natural frequencies are neglected for the same reasons for the aluminum beam and in Table 15. For the rotational coordinates the maximum value is 8.74E-07, there for a rotation is going to occur around the y-axis, the highest mass participation in the fifth row is 0.00011124 which is in the z-translation column. In the translational displacement as shown in Table 12, the beam will also rotate bout the y axis since the y-rotation has the highest effective mass value in the fifth mode row which is 8.74E-07 as shown in Table 15. There for the fifth mode shape is dominant thus the expected behavior is also bending since the translation through the z-axis and the rotation about the y-axis demonstrate bending. Regarding the electrical potential, the fifth mode shape is far higher than the first mode shape as shown in, Table 17 and for the magnesium beam in Table 11 the maximum mass participation on the translational x-axis column is 72.23% which demonstrate the dominance of the first mode. Following the first mode row the highest mass participation is 0.00122548 which in the z-translation column and in the rotational coordinate system in Table 14. The maximum value in the first mode row is 2.07E-05, thus the beam will exhibit bending behavior due to the combination of translation through the z-axis and rotating about the y-axis, and the third and fourth natural frequencies are neglected for the same reasons for the aluminum and titanium beams thus the expected response is also bending. Regarding the electrical peak electrical potential, the fifth mode produces higher electrical potential than the first mode as shown in Table 18. The fifth mode shape and the first mode shape and the second mode shape show bending and buckling behaviors due to the centrifugal force for all materials shown in Figure 45 and Figure 46 and Figure 47. Thus, the conclusion of the modal analysis is that the buckling behavior and the bending behavior are expected if the harmonic response analysis is done on the beams. The value of the electrical voltage produced will be around the fifth mode shape and the first mode shape.

Table 13: Aluminum and PZT-5H effective mass of rotational coordinates

Mode shape	x-Rotation	y-Rotation	z-Rotation
1	2.65E-08	2.69E-05	2.90E-13
2	4.39E-09	2.37E-06	1.17E-09
3	7.73E-10	1.06E-10	2.70E-05
4	1.31E-08	3.68E-11	6.46E-09
5	1.46E-09	6.71E-07	4.77E-13
Total effective mass	4.62E-08	3.00E-05	2.70E-05

Table 14: Magnesium and PZT-5H effective mass of rotational coordinates

Mode shape	x-Rotation	y-Rotation	z-Rotation
1	2.06E-08	2.07E-05	1.81E-13
2	3.87E-09	2.07E-06	1.14E-10
3	5.85E-10	1.16E-11	2.08E-05
4	9.80E-09	1.28E-11	1.27E-09
5	1.28E-09	5.88E-07	3.83E-14
Total effective mass	3.61E-08	2.34E-05	2.08E-05

Table 15: Titanium and PZT-5H effective mass of rotational coordinates

Mode shape	x-Rotation	y-Rotation	z-Rotation
1	4.20E-08	4.33E-05	2.89E-12
2	5.67E-09	3.13E-06	3.33E-12
3	2.11E-08	2.67E-10	4.44E-07
4	2.04E-09	3.59E-13	4.29E-05
5	1.92E-09	8.74E-07	7.89E-11
Total effective mass	7.27E-08	4.73E-05	4.34E-05

Table 16: Natural frequencies and peak electrical potential for Aluminum

Mode shape	Natural frequency	Electrical potential
1	65.4027	7.81E-07
2	621.876	5.36E-06
3	643.162	8.41E-07
4	875.738	2.49E-07
5	1814.17	1.39E-05

Table 17: Natural frequencies and peak electrical potential for Titanium

Mode shape	Natural frequency	Electrical potential
1	11.0354	1.61E-08
2	115.065	9.64E-08
3	146.69	-2.45E-08
4	269.68	1.96E-06
5	328.282	2.04E-07

Table 18: Natural frequencies and peak electrical potential for Magnesium

Mode shape	Natural frequency	Electrical potential
1	68.253	6.87E-07
2	607.919	4.76E-06
3	650.354	9.58E-07
4	930.736	2.42E-07
5	1781.14	1.23E-05

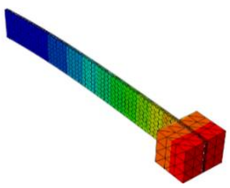

Mode shape 1

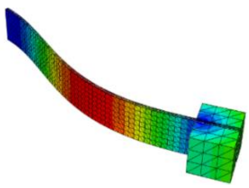

Mode shape 2

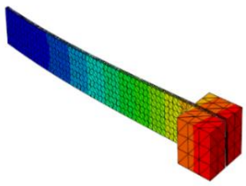

Mode shape 3

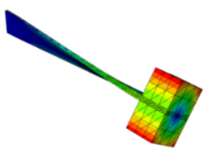

Mode shape 4

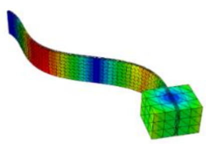

Mode shape 5

Figure 45: Mode shapes for aluminum substrate

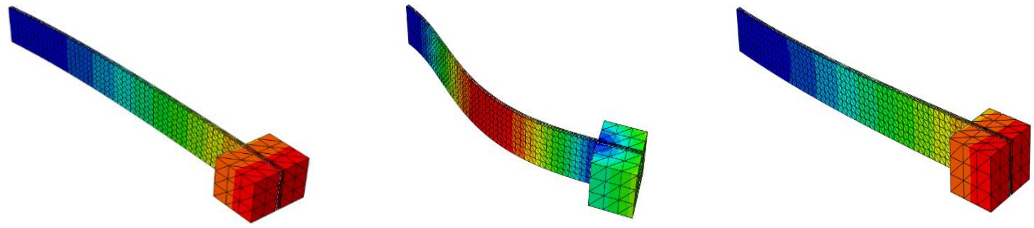

Mode shape 1 Mode shape 2 Mode shape 3

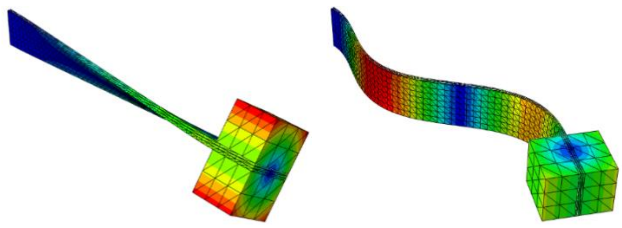

Mode shape 4 Mode shape 5

Figure 46: Mode shapes for magnesium substrate

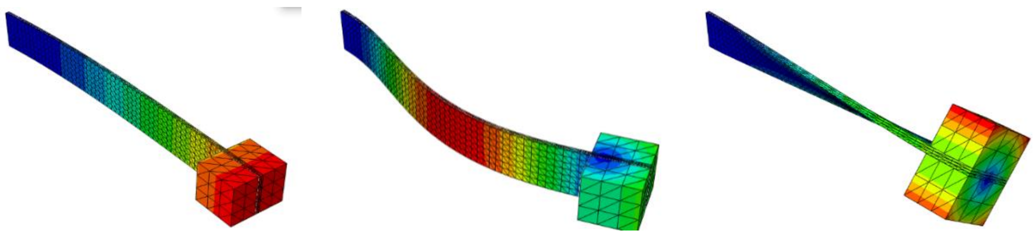

Mode shape 1 Mode shape 2 Mode shape 3

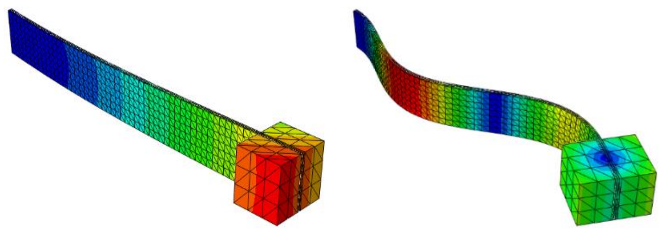

Mode shape 4 Mode shape 5

Figure 47: Mode shapes for Titanium and PZT-5H beam

4.2 Steady-State Analysis

The steady-state analysis is the process of obtaining the harmonic response due to a sinusoidal force in the frequency domain. Usually, this analysis is done to obtain the frequency where the maximum deflection happens which is called the resonance frequency. In energy harvesting, the ability to obtain the frequency that corresponds to maximum electrical potential is possible. The prerequisite for the steady-state analysis is the result of the modal analysis, since the expected mode needs to be known when applying a force in a certain direction at a certain frequency, as shown in Figure 48. The displacements of each beam demonstrated that the fifth mode of vibration is the dominating mode shape and then comes the first mode shape.as predicted from model analysis.

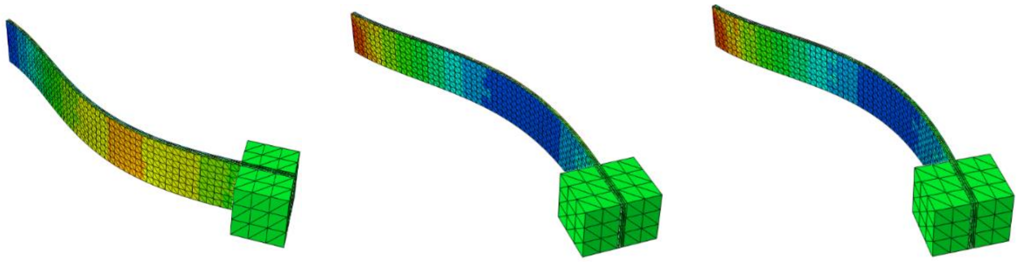

Aluminum and PZT-5H beam | Magnesium and PZT-5H beam | Titanium and PZT-5H beam

Figure 48: The harmonic response for each beam

The harmonic response concludes that Magnesium has the top resonance frequency in terms of voltage with a value of 250.0 Hz and then Aluminum comes next with the value of 240.0 Hz and the least is titanium with a value of 40.0 Hz. Table 19 shows the top voltage for each beam since the magnesium has the highest produced electrical potential then the magnesium will have the maximum power output as shown in Table 19. The noise inherited in each beam showed a remarkable increase in the output voltage in each beam from the Nano-volts range to the range of the volt as shown in Table 20 and since the magnesium is the highest voltage then the highest output power will be magnesium as shown in Table 21.

Table 19: Summary of the voltages of beams without noise

Material and piezoelectric material	Noised maximum voltage output
Aluminum + PZT-5H	4 pV
Magnesium+ PZT-5H	8.0 pV
Titanium + PZT-5H	2 pV

Table 20: Voltage output after noise inheritance

Material and piezoelectric material	Maximum voltage output after noise inheritance
Aluminum + PZT-5H	5.8561 V
Magnesium+ PZT-5H	7.2749 V
Titanium + PZT-5H	5.9273 V

Table 21: Summary of the power output for each model

Material and piezoelectric material	Maximum power output
Substrata + PZT-5J	370μW
Aluminum + PZT-5H	489.92 μW
Magnesium+ PZT-5H	756.06 μW
Titanium + PZT-5H	501.9 μW

4.3 Temperature Effect on the Power Output

The temperature influences the young's modulus for normal metals and dielectric constant and coupling factor along with the young's modulus for PZT-5H. Thus, experimental data should be collected and curve fitted to get a general equation out of it so the material properties are predicted as the desired temperature range which is from 50°C to 150°C. The modal and harmonic analysis are done on the temperature range with a step size of 10°C. Regarding the modal analysis, the mode shapes of aluminum and magnesium are no different from the mode shape without temperature effect, however, titanium mode shapes changes at 150°C where the second mode shape exchanged places with the third mode shape. Since the thermal deformation in titanium beam is higher than aluminum and magnesium beam, the mode shapes are shown in Figures 49-51 for aluminum, then Figures 52-54 for magnesium, then Figure 55-57 for titanium. The modal effective mass values are not affected by temperature where for aluminum and titanium where the fifth mode is always dominant on all temperatures where in Table 22 mode shape five participates with 50.90%, in Table 24. The fifth mode participates with 58.69% and Table 26 the fifth mode participates with 60.40% from the total effective mass in the x-translation and for titanium in Table 34 and Table 28 the fifth mode participate with 67.14%. In Table 36 the fifth mode participates with 65.57%, in Table 38 the fifth mode participates with 64.57% from the total effective mass in x-translation. However, in magnesium the first mode shape became dominant in the temperature above 100°C where in Table 28 the first mode dominates with 76.89% and Table 30 the first mode participates with 48.04% of the total effective mass in x-translation. In Table 32 the fifth mode participates with 66.48% of the total mass in the x-translation.

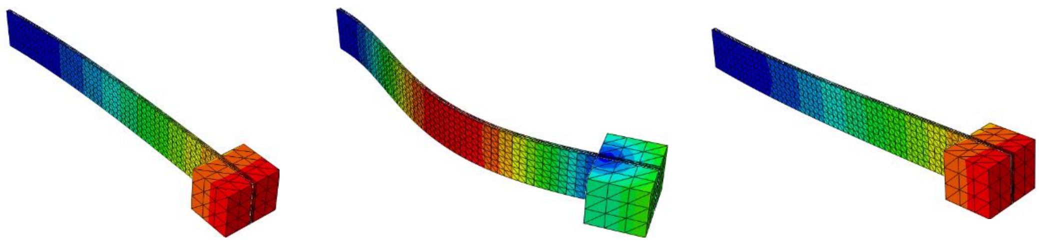

Mode shape 1 Mode shape 2 Mode shape 3

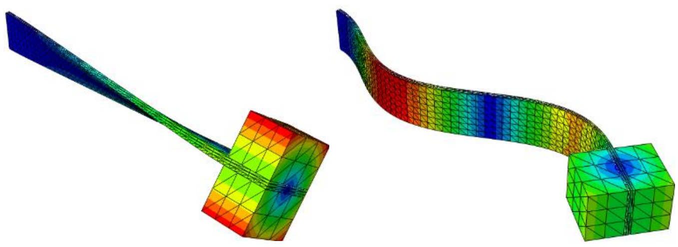

Mode shape 4 Mode shape 5

Figure 49: Mode shapes foe aluminum and PZT-5H at 50°C

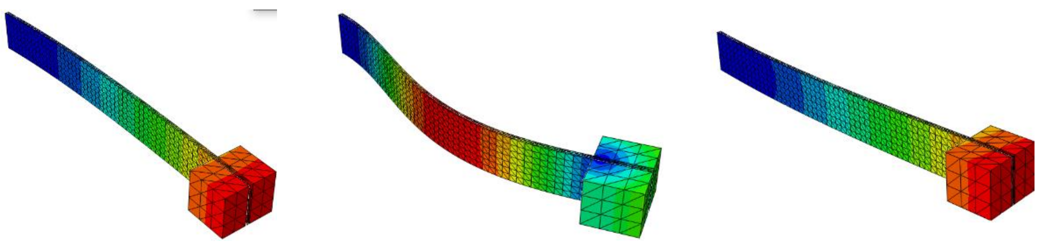

Mode shape 1 Mode shape 2 Mode shape 3

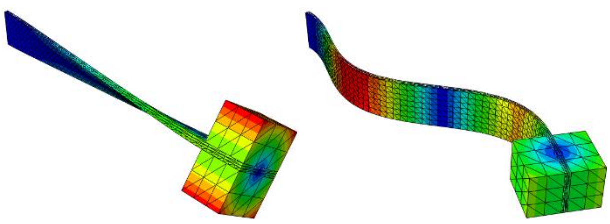

Mode shape 4 Mode shape 5

Figure 50: Mode shapes foe aluminum and PZT-5H at 100°C

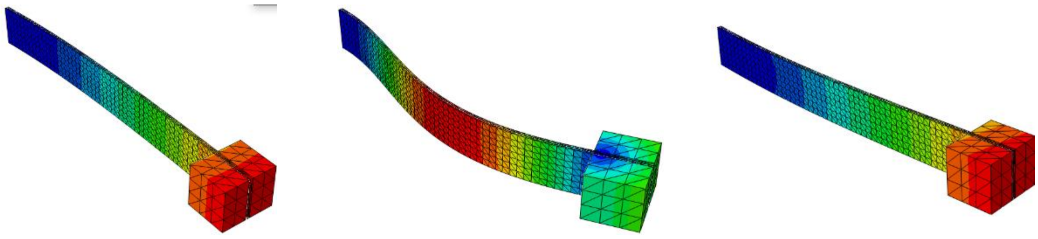

Mode shape 1 Mode shape 2 Mode shape 3

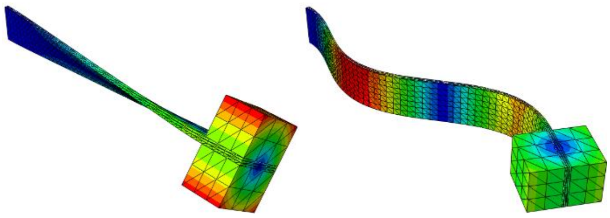

Mode shape 4 Mode shape 5

Figure 51: Mode shapes foe aluminum and PZT-5H at 150°C

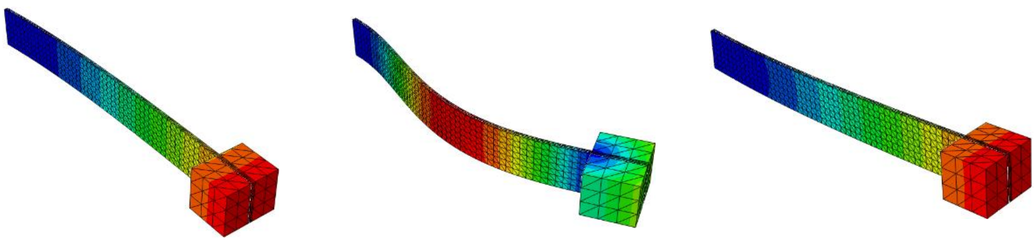

Mode shape 1 Mode shape 2 Mode shape 3

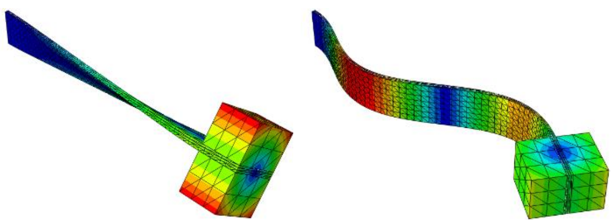

Mode shape 4 Mode shape 5

Figure 52: Mode shapes foe magnesium and PZT-5H at 50°C

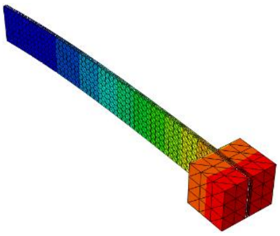

Mode shape 1

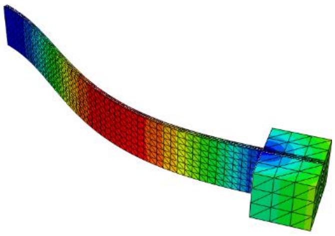

Mode shape 2

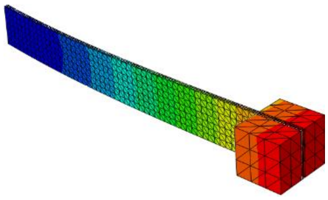

Mode shape 3

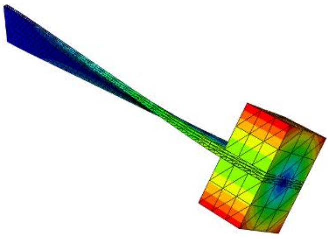

Mode shape 4

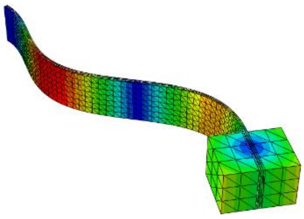

Mode shape 5

Figure 53: Mode shapes foe magnesium and PZT-5H at 100°C

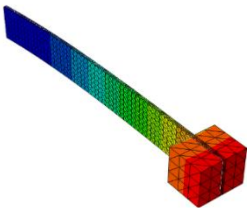

Mode shape 1

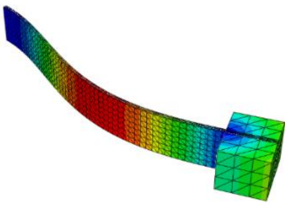

Mode shape 2

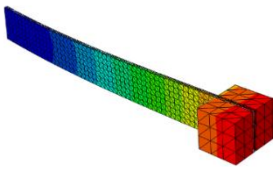

Mode shape 3

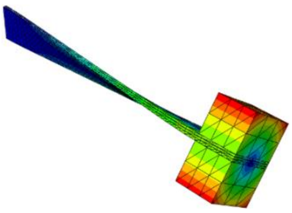

Mode shape 4

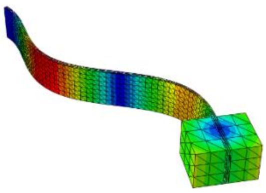

Mode shape 5

Figure 54: Mode shapes foe magnesium and PZT-5H at 150°C

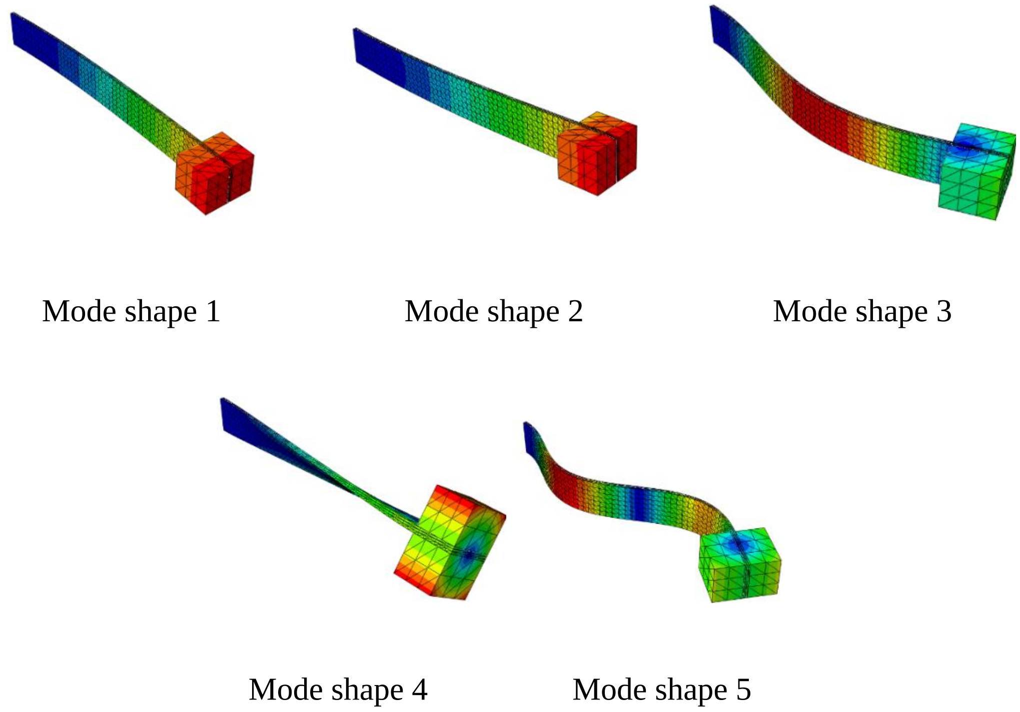

Figure 55: Mode shapes for titanium and PZT-5H at 50°C

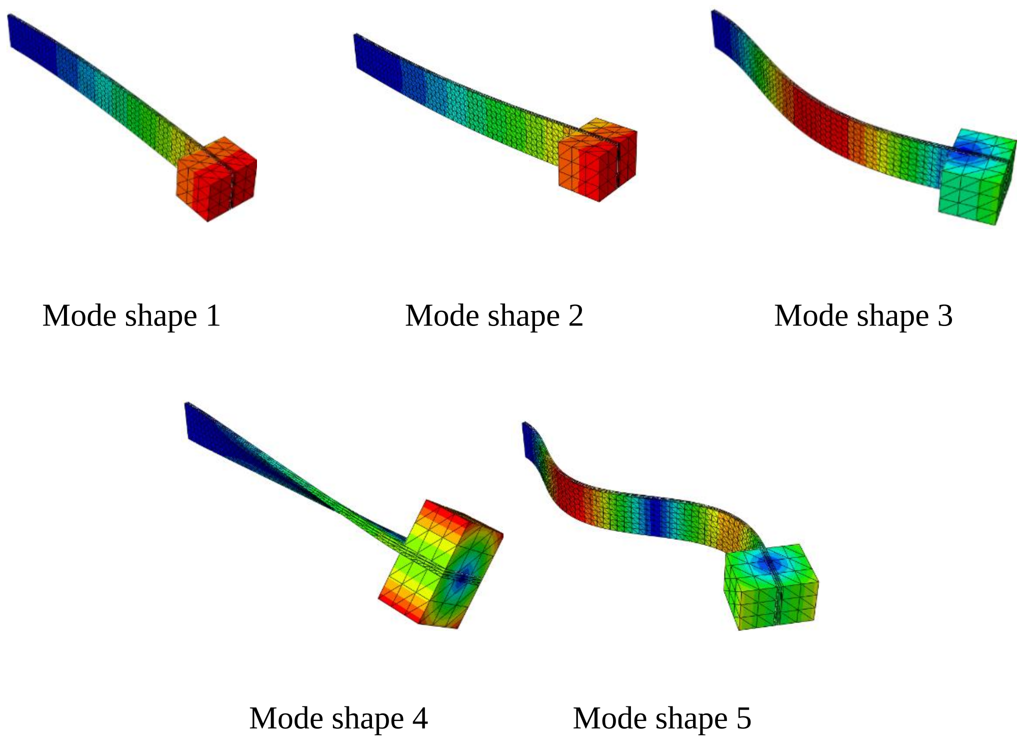

Figure 56: Mode shapes foe titanium and PZT-5H at 100°C

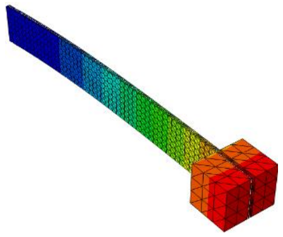

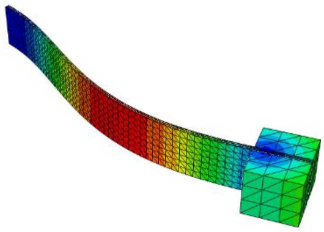

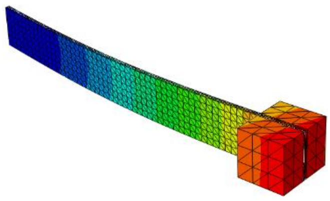

Mode shape 1 Mode shape 2 Mode shape 3

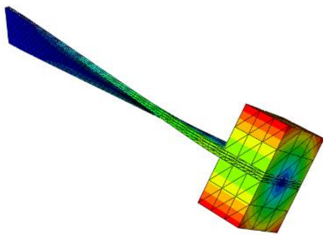

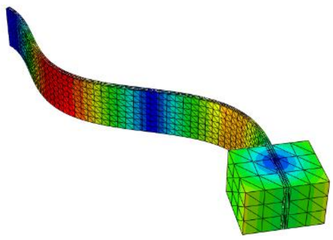

Mode shape 4 Mode shape 5

Figure 57: Mode shapes foe titanium and PZT-5H at 150°C

Table 22: Modal effective mass for aluminum substrate and PZT-5H at 50°C in translation coordinates

Mode shape	x-Translation	y-Translation	z-Translation
1	4.12E-09	1.64E-12	0.00157607
2	2.42E-09	6.12E-07	0.00026715
3	2.98E-13	0.00158096	1.03E-07
4	3.77E-16	4.82E-08	3.07E-09
5	6.77E-09	5.34E-13	8.55E-05
Total effective mass	1.33E-08	1.58E-03	1.93E-03

Table 23: Modal effective mass for aluminum substrate and PZT-5H in rotational coordinates at 50°C

Mode shape	x-Rotation	y-Rotation	z-Rotation
1	2.65E-08	2.69E-05	1.80E-13
2	4.34E-09	2.37E-06	1.04E-08
3	7.64E-10	9.12E-10	2.70E-05
4	1.32E-08	3.54E-11	1.27E-09
5	1.46E-09	6.70E-07	6.60E-14
Total effective mass	4.62E-08	3.00E-05	2.70E-05

Table 24: Modal effective mass for aluminum substrate and PZT-5H at 100°C in translation coordinates

Mode shape	x-Translation	y-Translation	z-Translation
1	8.10E-09	1.81E-12	0.00157604
2	1.41E-08	7.18E-08	0.000267299
3	9.39E-14	0.0015812	1.20E-08
4	2.36E-13	3.05E-07	3.15E-09
5	3.15E-08	1.21E-12	8.55E-05
Total effective mass	5.37E-08	1.58E-03	1.93E-03

Table 25: Modal effective mass for aluminum substrate and PZT-5H in rotational coordinates at 100°C

Mode shape	x-Rotation	y-Rotation	z-Rotation
1	2.65E-08	2.69E-05	2.89E-13
2	4.39E-09	2.37E-06	1.19E-09
3	7.73E-10	1.08E-10	2.70E-05
4	1.31E-08	3.68E-11	6.38E-09
5	1.46E-09	6.71E-07	4.71E-13
Total effective mass	4.62E-08	3.00E-05	2.70E-05

Table 26: Modal effective mass for aluminum substrate and PZT-5H at 150°C in translation coordinates

Mode shape	x-Translation	y-Translation	z-Translation
1	2.08E-08	2.66E-12	2.50E-03
2	1.53E-07	6.94E-08	3.52E-04
3	1.79E-12	2.50E-03	1.08E-08
4	1.13E-11	7.76E-06	1.39E-08
5	3.18E-07	3.77E-12	1.13E-04
Total effective mass	4.92E-07	2.51E-03	2.96E-03

Table 27: Modal effective mass for aluminum substrate and PZT-5H in rotational coordinates at 150°C

Mode shape	x-Rotation	y-Rotation	z-Rotation
1	4.20E-08	4.33E-05	6.35E-13
2	5.71E-09	3.13E-06	1.08E-09
3	1.58E-09	9.89E-11	4.32E-05
4	2.16E-08	1.51E-10	1.39E-07
5	1.93E-09	8.87E-07	5.56E-12
Total effective mass	7.28E-08	4.73E-05	4.34E-05

Table 28: Modal effective mass for magnesium substrate and PZT-5H at 50°C in translation coordinates

Mode shape	x-Translation	y-Translation	z-Translation
1	1.05E-09	1.01E-12	0.00122551
2	2.99E-09	6.05E-09	0.000234011
3	4.15E-14	0.0012298	1.08E-09
4	8.55E-15	1.30E-08	9.48E-10
5	8.02E-09	1.11E-12	7.52E-05
Total effective mass	1.21E-08	1.23E-03	1.53E-03

Table 29: Modal effective mass for magnesium substrate and PZT-5H in rotational coordinates at 50°C

Mode shape	x-Rotation	y-Rotation	z-Rotation
1	2.06E-08	2.07E-05	6.65E-14
2	3.88E-09	2.07E-06	1.06E-10
3	5.38E-10	9.80E-12	2.08E-05
4	9.84E-09	1.23E-11	5.18E-11
5	1.28E-09	5.87E-07	1.24E-13
Total effective mass	3.61E-08	2.34E-05	2.08E-05

Table 30: Modal effective mass for magnesium substrate and PZT-5H at 100°C in translation coordinates

Mode shape	x-Translation	y-Translation	z-Translation
1	2.67E-09	1.18E-12	0.00122549
2	9.54E-11	7.19E-09	0.000234037
3	2.25E-14	0.0012298	1.30E-09
4	1.03E-13	2.50E-09	9.54E-10
5	7.06E-10	1.95E-12	7.52E-05
Total effective mass	3.47E-09	1.23E-03	1.53E-03

Table 31: Modal effective mass for magnesium substrate and PZT-5H in rotational coordinates at 100°C

Mode shape	x-Rotation	y-Rotation	z-Rotation
1	2.06E-08	2.07E-05	1.20E-13
2	3.87E-09	2.07E-06	1.21E-10
3	5.62E-10	1.18E-11	2.08E-05
4	9.82E-09	1.25E-11	2.17E-10
5	1.28E-09	5.88E-07	3.98E-15
Total effective mass	3.61E-08	2.34E-05	2.08E-05

Table 32: Modal effective mass for magnesium substrate and PZT-5H at 150°C in translation coordinates

Mode shape	x-Translation	y-Translation	z-Translation
1	6.21E-09	1.43E-12	0.00122547
2	2.88E-09	6.49E-09	0.00023408
3	3.95E-15	0.00122969	1.18E-09
4	4.36E-13	9.25E-08	9.73E-10
5	3.84E-09	3.39E-12	7.52E-05
Total effective mass	1.29E-08	1.23E-03	1.53E-03

Table 33: Modal effective mass for magnesium substrate and PZT-5H in rotational coordinates at 150°C

Mode shape	x-Rotation	y-Rotation	z-Rotation
1	2.06E-08	2.07E-05	2.21E-13
2	3.87E-09	2.07E-06	1.03E-10
3	5.99E-10	1.08E-11	2.08E-05
4	9.78E-09	1.30E-11	2.36E-09
5	1.28E-09	5.88E-07	1.17E-13
Total effective mass	3.61E-08	2.34E-05	2.08E-05

Table 34: Modal effective mass for titanium substrate and PZT-5H at 50°C in translation coordinates

Mode shape	x-Translation	y-Translation	z-Translation
1	7.56E-09	2.23E-12	2.50E-03
2	3.79E-12	2.51E-03	1.31E-08
3	4.21E-08	9.44E-08	3.52E-04
4	1.41E-12	7.13E-07	1.35E-08
5	1.01E-07	9.58E-13	1.12E-04
Total effective mass	1.51E-07	2.51E-03	2.96E-03

Table 35: Modal effective mass for titanium substrate and PZT-5H in rotational coordinates at 50°C

Mode shape	x-Rotation	y-Rotation	z-Rotation
1	4.20E-08	4.33E-05	3.00E-13
2	1.09E-09	1.15E-10	4.34E-05
3	5.77E-09	3.13E-06	1.71E-09
4	2.20E-08	1.43E-10	1.34E-08
5	1.92E-09	8.85E-07	1.51E-12
Total effective mass	7.28E-08	4.73E-05	4.34E-05

Table 36: Modal effective mass for titanium substrate and PZT-5H at 100°C in translation coordinates

Mode shape	x-Translation	y-Translation	z-Translation
1	1.28E-08	2.38E-12	2.50E-03
2	3.41E-10	2.50E-03	1.31E-06
3	8.38E-08	9.36E-06	3.51E-04
4	4.37E-12	2.14E-06	1.38E-08
5	1.85E-07	1.87E-12	1.12E-04
Total effective mass	2.82E-07	2.51E-03	2.96E-03

Table 37: Modal effective mass for titanium substrate and PZT-5H in rotational coordinates at 100°C

Mode shape	x-Rotation	y-Rotation	z-Rotation
1	4.20E-08	4.33E-05	4.35E-13
2	9.43E-10	1.16E-08	4.32E-05
3	6.05E-09	3.12E-06	1.63E-07
4	2.19E-08	1.47E-10	3.91E-08
5	1.92E-09	8.86E-07	3.02E-12
Total effective mass	7.28E-08	4.73E-05	4.34E-05

Table 38: Modal effective mass for titanium substrate and PZT-5H at 150°C in translation coordinates

Mode shape	x-Translation	y-Translation	z-Translation
1	2.08E-08	2.66E-12	2.50E-03
2	1.53E-07	6.94E-08	3.52E-04
3	1.79E-12	2.50E-03	1.08E-08
4	1.13E-11	7.76E-06	1.39E-08
5	3.18E-07	3.77E-12	1.13E-04
Total effective mass	4.92E-07	2.51E-03	2.96E-03

Table 39: Modal effective mass for titanium substrate and PZT-5H in rotational coordinates at 150°C

Mode shape	x-Rotation	y-Rotation	z-Rotation
1	4.20E-08	4.33E-05	6.35E-13
2	5.71E-09	3.13E-06	1.08E-09
3	1.58E-09	9.89E-11	4.32E-05
4	2.16E-08	1.51E-10	1.39E-07
5	1.93E-09	8.87E-07	5.56E-12
Total effective mass	7.28E-08	4.73E-05	4.34E-05

Regarding the harmonic analysis, for aluminum the deformation behavior stays the same with the temperature up to a threshold is then the deformation behavior changes permanently however this is not the case for magnesium and titanium, the deformation behavior of all beams at 50°C and 100°C and 150°C is Figures 58-60 The curve fittings for young's modulus versus temperature are Figures 61 - 63for aluminum and titanium and magnesium. The curve fittings of young's modulus versus temperature and dielectric constant versus temperature and coupling factor versus temperature for PZT-5H are shown in Figures 64-66, to demonstrate and quantify the quality of the fit, a certain quantity should be investigated which is R-squared, R-squared is calculated by the following formula.

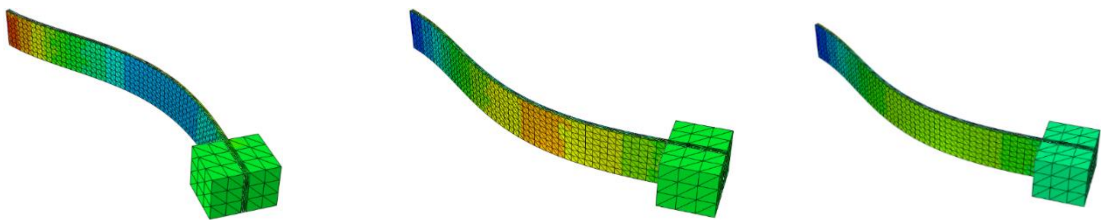

Aluminum deformation at 50°C

Aluminum deformation at 100°C

Aluminum deformation at 150°C

Figure 58: Aluminum substrate and PZT-5H deformation behavior at different temperatures

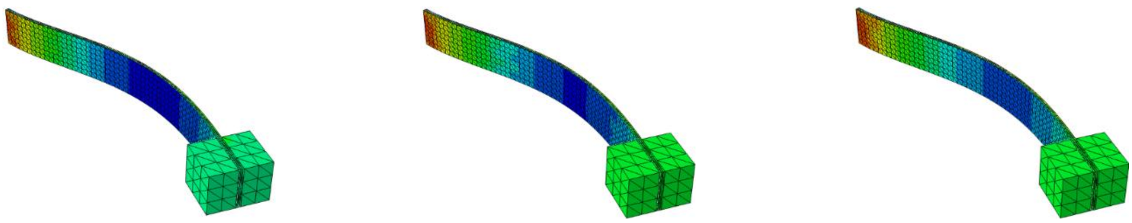

Magnesium deformation at 50°C

Magnesium deformation at 100°C

Magnesium deformation at 150°C

Figure 59: Magnesium substrate and PZT-5H deformation behavior at different temperatures

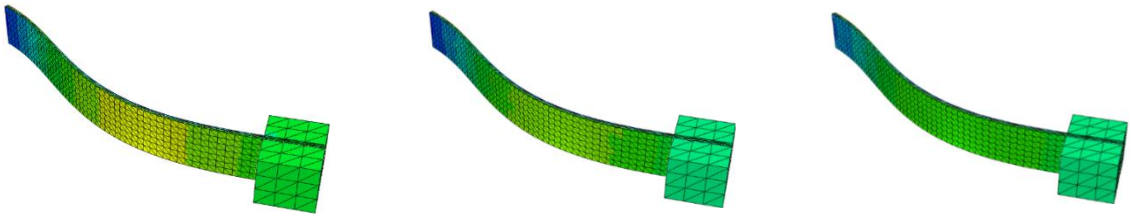

Titanium deformation at 50°C | Titanium deformation at 100°C | Titanium deformation at 150°C

Figure 60: Titanium substrate and PZT-5H deformation behavior at different temperature

$$R^2 = \frac{var(mean) - var(chosen\ curve)}{var(mean)} \quad (1)$$

Where var(mean) is the is the squared difference from the actual data value form the mean which the average of the whole data point. The mean is a straight horizontal line fitting the data. Var (chosen curve) which the squared difference between the actual data points and the chosen curve that best fit the data. The range of R square is from zero to one, the closer the R square to one the better. The “cftool” in MATLAB® can automatically calculate the R squared values, the R squared values shows a remarkable value for each material. Table 40 shows the curve fitting results along with the R squared values for each material.

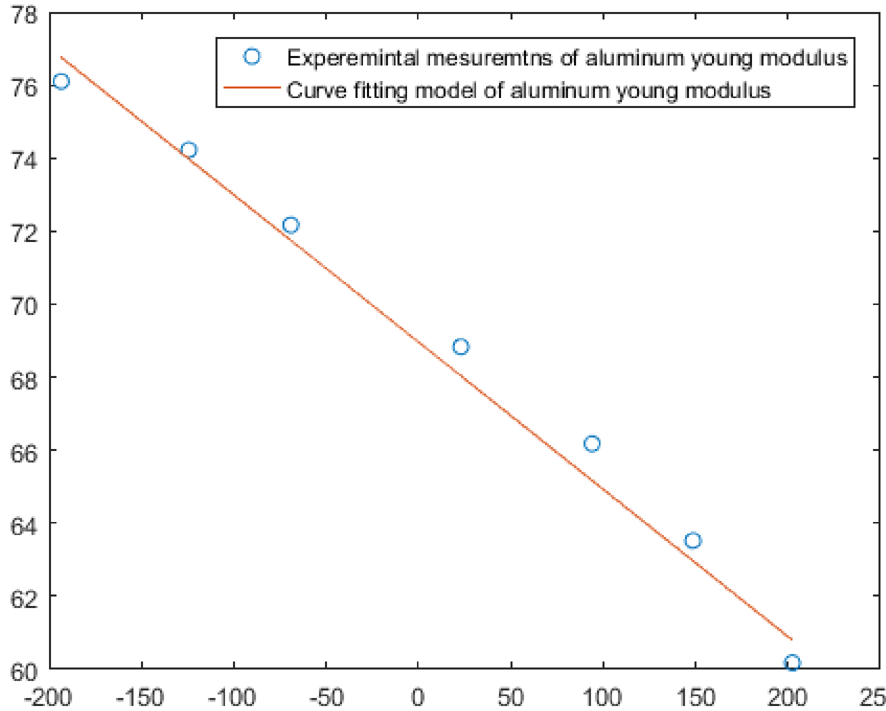

Figure 61: Young's modulus versus temprature for Aluminum the data are from [54]

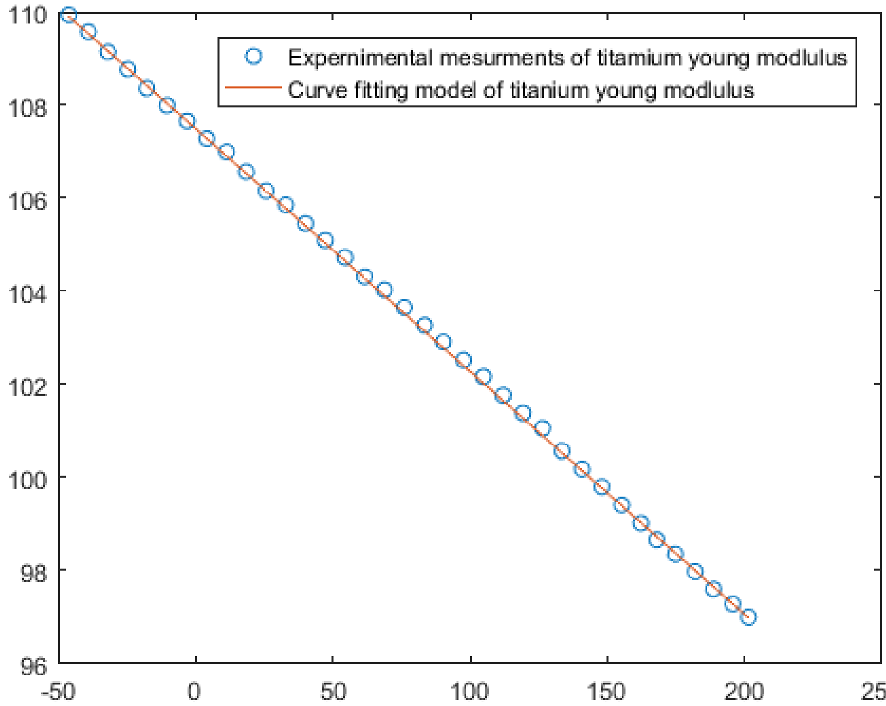

Figure 62: Young’s modulus versus temperature fitting for Titanium the data are from [56]

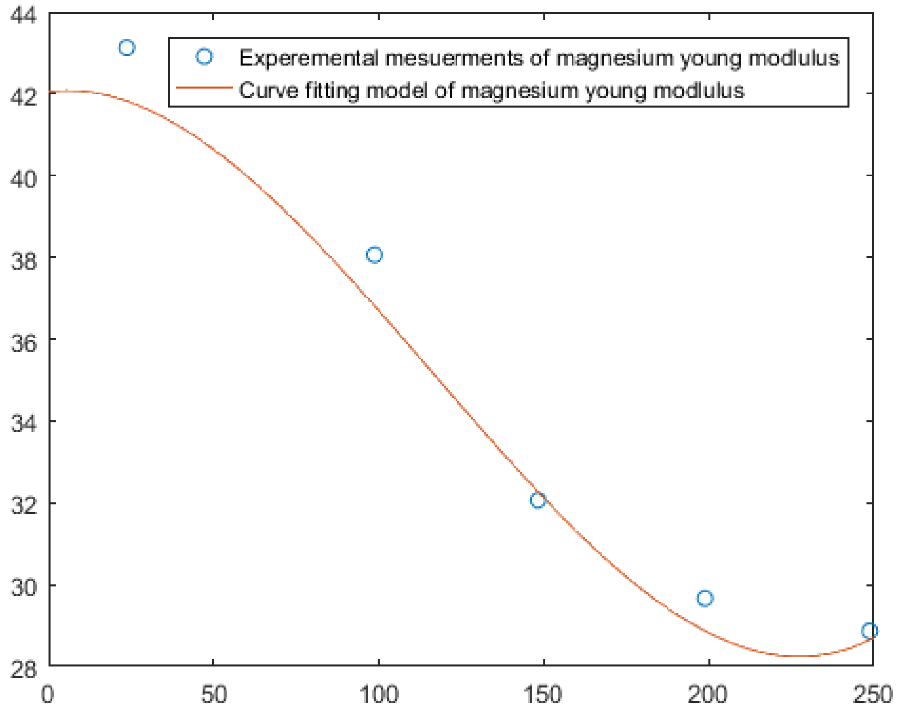

Figure 63: Young's modulus versus temperature fitting for Magnesium the data are from [58]

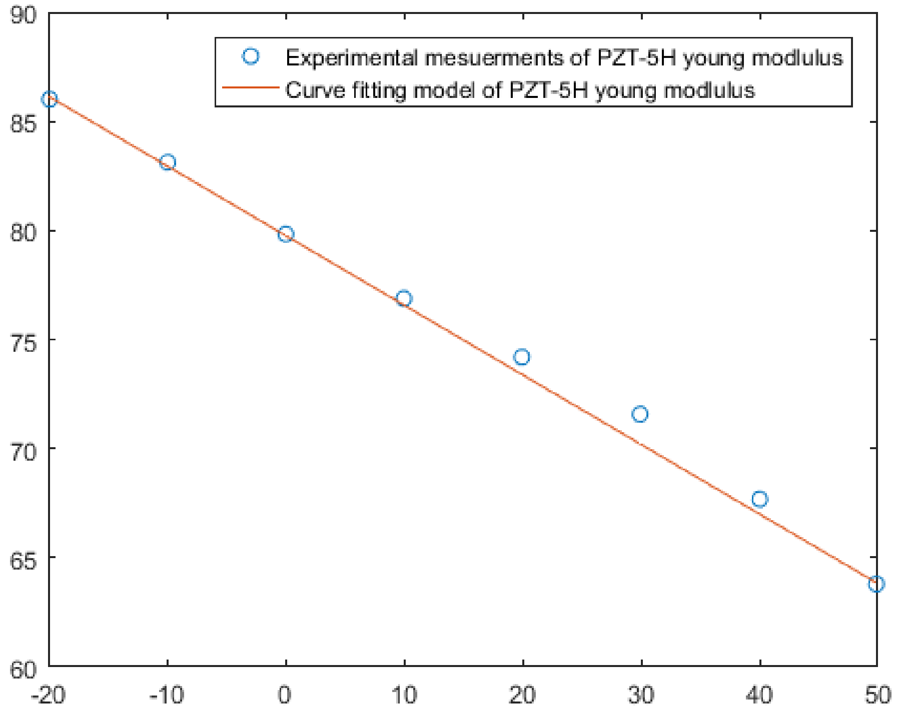

Figure 64: Young’s modulus versus temperature for PZT-5H the data are from [57]

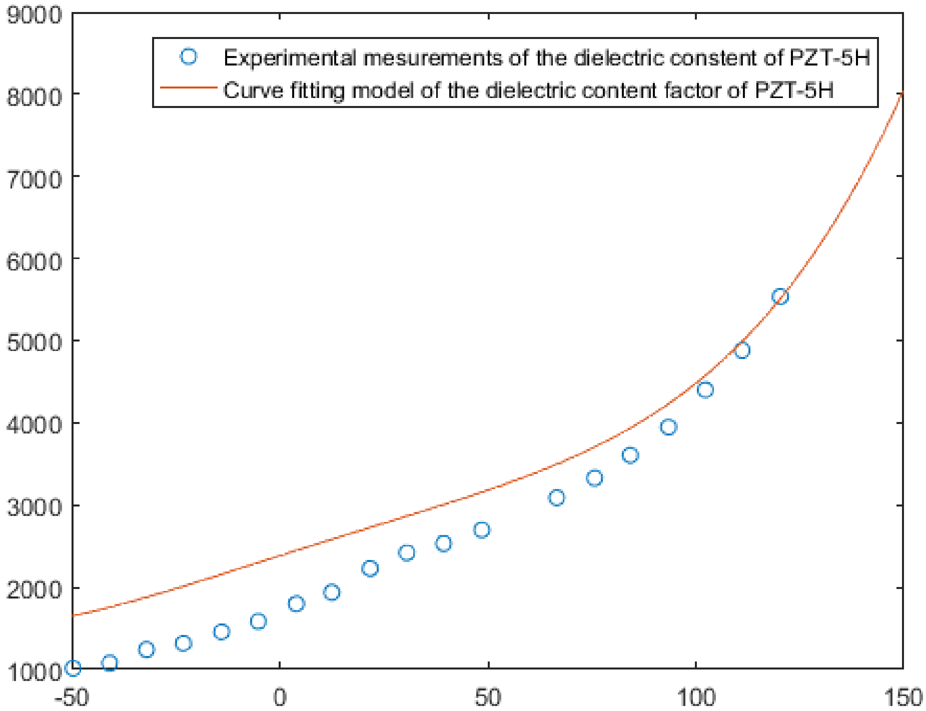

Figure 65: Dielectric constant versus temperature for PZT-5H the data are from [57]

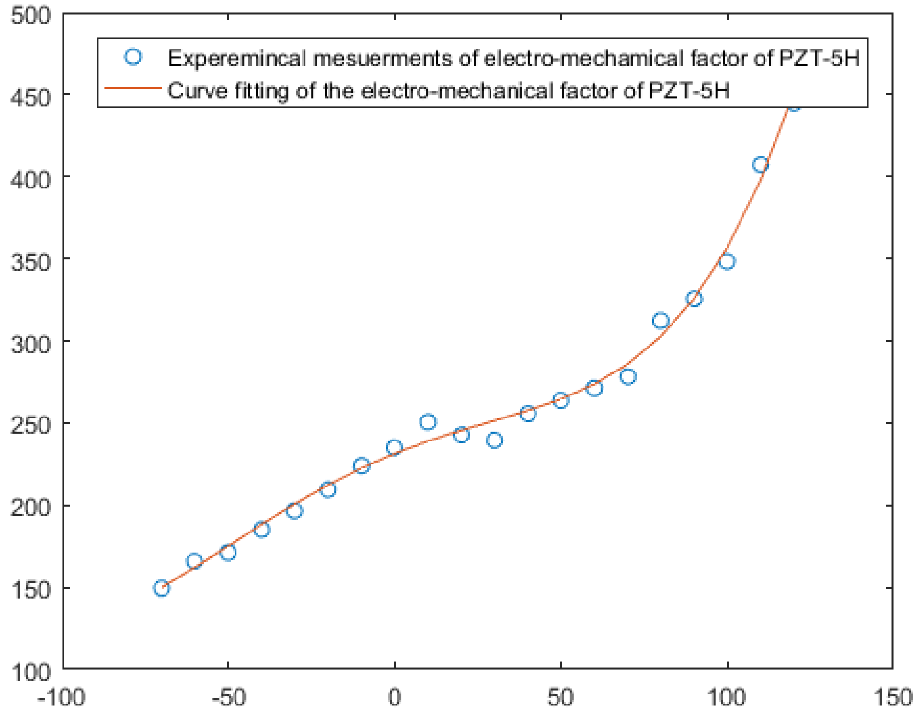

Figure 66: Coupling factor versus temperature for PZT-5H data are from [57]

Table 40: Curve fitting results

Material	Fitting type	Quantity versus temperature	Fitting formula	Constant values	R-Squared
PZT-5H	Polynomial	Young's modulus	p_1x+p_2	p_1= 0.319 p_2=79.77	0.9966
PZT-5H	Polynomial	Dielectric constant	$P_1x^4+p_2x^3+p_3x^2+p_4x+p_5$	P_1= 8.935e-06 p_2=0.0003127 p_3=0.009363 p_4 =16.1 p_5=2383	0.9993
PZT-5H	Polynomial	Coupling factor	$P_1x^4+p_2x^3+p_3x^2+p_4x+p_5$	p_1=7.817e07 p_2=3.144e05 p_3=0.006574 p_4=0.8154 p_5=231.4	0.9937
Aluminum	Polynomial	Young's modulus	p_1x+p_2	p_1 = -0.04032 p_2 = 68.96	0.9878
Titanium	Polynomial	Young's modulus	p_1x+p_2	p_1 = -0.05219 p_2 = 107.5	0.9998
Magnesium	Polynomial	Young's modulus	$p_1x^3+p_2x^2+p_3x+p_4$	p_1=2.542e-06 p_2=0.0008884 p_3 = 0.00981 p_4 = 42.06	0.9935

The results of harmonic analysis under the temperature showed that the electrical potential increases with the increase of the temperature up to a particular point and then the voltage drop with the increase of temperature. Figure 67 showing the electrical potential behavior with no white noise added for each beam with the increase of temperature. Where as shown in Figure 67a aluminum's electrical potential skyrockets at 70 °C wherein Figure 67b for the titanium the electrical potential increases slowly and in magnesium the electrical potential decreases with temperature from 50°C as shown in Figure 67c. This behavior is due to the fact that the young's modulus is decreasing with the increase of temperature for all materials and since the young's modulus is proportional to the natural frequency of the cantilever beams, this means that the maximum deformation due to vibration will decrease with the increase of temperature. However the dielectric constant and the electro-mechanical coupling factor are proportional with the temperature which shows why the electrical potential increases with temperature for aluminum and titanium in Figure 67a and Figure 67b because the temperature decreases linearly as shown Figures 61-62. But for magnesium the temperature decreases nonlinearly as shown in Figure 63 which shows the voltage potential is decreasing with temperature in Figure 67c. The results of calculating the power output at the temperature where the voltage is the highest. Table 41 shows the power output compared with the power output without temperature after adding the white noise. This shows that the temperature is a game-changer wherein harmonic analysis without the temperature magnesium was the highest but once the temperature is considered the aluminum became the highest producing power. But the power produced with the temperature was less than the power produced without the temperature however the difference is not far which conclude that the temperature might have a negative effect on the produced power.

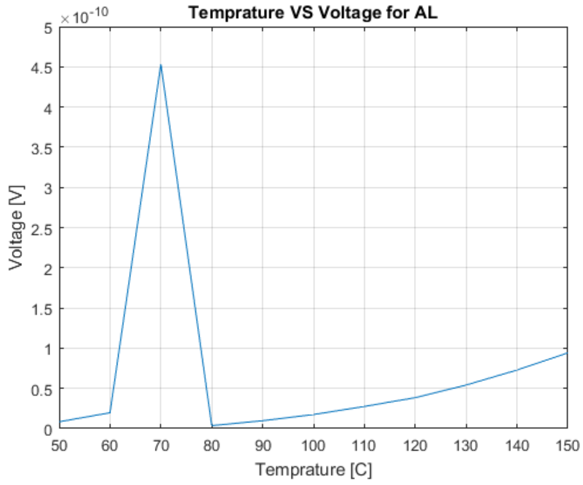

(a)

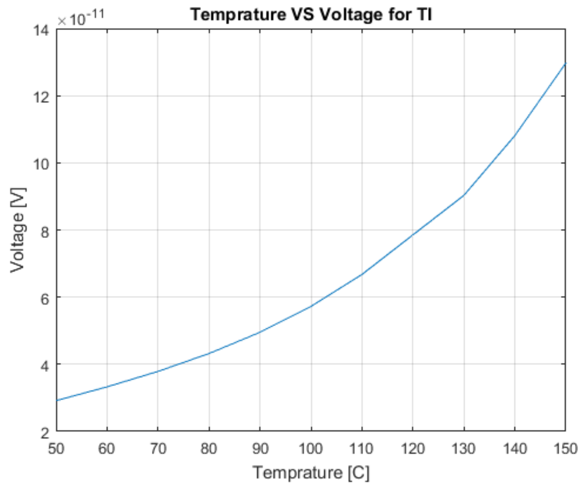

(b)

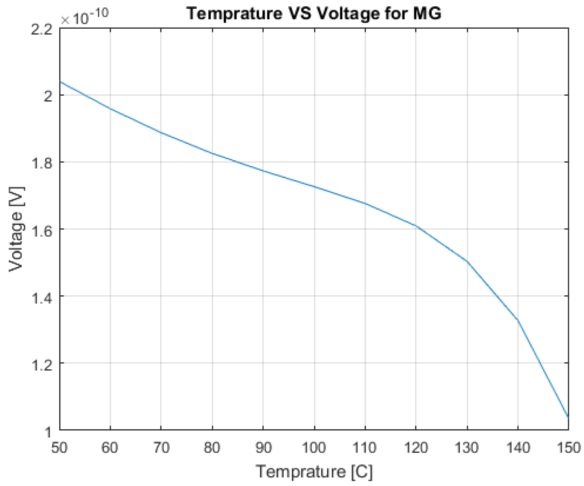

(c)

Figure 67: Electrical potential versus temperature for each beam's substrate

Table 41: Power output comparison for with and without temperature

Beam	Power output with temperature	Power output without temperature
Aluminum	427 μW	489.92 μW
Magnesium	401 μW	756.06 μW
Titanium	395 μW	501.9 μW

4.4 Discussion

From the obtained results, noised environment proved to be useful where the voltages increased significantly where the voltage of the three energy harvesters was in the Pico-volt range before the noise inheritance, but after adding the noise the voltage of the harvesters became in the volt range. The power output with noise form the three harvesters exceeded the results obtained from Gustav et al [54]. This proved that lightweight material substrates could increase the electrical power output. The temperature effected the power output of the harvesters by effecting the elastic modulus and volume of all harvesters, since each material has different response to temperature. Which led to the aluminum and PZT-5H beam to achieve the highest power output, since aluminum is a good electrical and thermal transmitter, since temperature decreases the elastic modulus, the overall power output is lower than the overall power output without temperature. Where the least power output without temperature is 489.92 μW and the maximum power output with temperature was 427.0 μW.

4.5 Summary of the Chapter

In this chapter the results of vibrational analysis for three PZT-5H beams each with a different substrate are discussed. The analysis is divided into four parts, the first one is the modal analysis where the possible responses of the system are obtained, each response has its effective mass value and corresponding electrical potential since the piezoelectric material produces energy when deformed. Each response also has a sweet spot and natural frequency for the response to appear on the structure. The second part of vibration analysis is steady-state analysis, also known as a harmonic response or frequency response. The applied boundary force are sinusoidal due to the nature of the vibrating environment harmonic analysis are required and the third part was the noise inheritance to the harmonic response where the harmonic response is shifted to time domain using "ifft" command in MATLAB® and the white noise was added. The results was transferred back to frequency domain using "fft" command in MATLAB®. The fourth part was temperature effect where experimental data are obtained from four papers, the first three papers measures the young's modulus versus temperature for aluminum and magnesium and titanium. The fourth paper measured the dielectric constant and the coupling factor and the young's modulus for PZT-5H all versus temperature. Curve fitting sessions where curried out using "cftool" command in MATLAB® to obtain the formulas between the materials properties and the temperature to predict the material properties at the temperature range from 50°C to 150°C with 10°C in step size. The harmonic analysis was carried out with the obtained material properties, the analysis concluded that the beams took the first and fifth mode responses and the top produced power was magnesium and then comes the aluminum and then comes titanium. And the temperature has a negative effect on the produced power where the power was less than the power without the temperature effect however the difference was not very high.

Chapter 5

CONCLUSION

In this thesis, background information about piezoelectric material was given and the energy harvesting concept was also discussed. The key contributions and aims are presented. A comprehensive literature review about piezoelectric rotating energy harvester was presented, the literature review included the simulation technique and beam designs employed and the piezoelectric material employed in energy harvesting. The review concluded that the research gap was the employment of light material beams and employing of FEM, and considering the noise and temperature effect on the piezoelectric energy harvesters. The research methodology applied in this thesis was presented which was a comparative study of the produced power between three harvesters similar to Gustav et al except that the substrate for each beam were aluminum and magnesium and titanium since they are considered to be light weight and strong. But all of these beams have the same piezoelectric material which is PZT-5H since it has a higher capacity for producing electrical potential. The comparative study was to conduct vibration analysis on the beams to obtain their resonance frequency and add noise to the result and then temperature effect was investigated to see the behavior of the produced power from each harvester. The analysis was done using ABAQUS® software. The geometry, material setting, boundary conditions were explained and illustrated. Next the results of the vibration analysis were presented, the results concluded:

- PZT-5H produced higher electrical output than PZT-5J.

- Noise proved to be very useful where the voltage increased significantly with noise inheritance.
- the model analysis concluded that the buckling behavior would be the dominant behavior in the beam.
- Magnesium substrate PZT-5H produced the highest electrical power.
- Temperature proved to be a game-changer for the aluminum and the PZT-5H beam had the highest electrical power.
- Overall electrical power with the temperature is less than the overall power generated without the temperature.

REFERENCES

[1] Sensorics P. *Fundamentals of Piezoelectric Sensorics Mechanical, Dielectric, and Thermodynamical Properties of Piezoelectric Materials*.pdf. London, New York: Springer; n.d. https://doi.org/10.1007/978-3-540-68427-5.

[2] Uchino K, Debus JC. *Advanced piezoelecgtric materials.* 2cd ed. *Elsevier Ltd*; 2017. https://doi.org/10.1533/9780857096319.

[3] Kilner JA, Skinner SJ, Irvine SJC, Edwards PP. *Functional materials for sustainable energy applications*. 2012. https://doi.org/10.1533/9780857096371.

[4] Hung PK, Vinh LT, Nghiep DM, Nguyen PN. *Computer simulation of liquid Al2O3. J Phys Condens Matter* 2006;18:9309–22. https://doi.org/10.1088/0953-8984/18/41/001.

[5] Zhang J, Fang Z, Shu C, Zhang J, Zhang Q, Li C. *A rotational piezoelectric energy harvester for efficient wind energy harvesting*. *Sensors Actuators*, A Phys 2017;262:123–9. https://doi.org/10.1016/j.sna.2017.05.027.

[6] Rui X, Zhang Y, Zeng Z, Yue G, Huang X, Li J. *Design and analysis of a broadband three-beam impact piezoelectric energy harvester for low-frequency rotational motion. Mech Syst Signal Process* 2021;149:107307. https://doi.org/10.1016/j.ymssp.2020.107307.

[7] Guan M, Liao WH. *Design and analysis of a piezoelectric energy harvester for rotational motion system*. *Energy Convers Manag* 2016;111:239–44. https://doi.org/10.1016/j.enconman.2015.12.061.

[8] Raja V, Umapathy M, Uma G, Praveen Kumar B, Premkumar S. *Design, analysis and experimental investigation of a rotational piezoelectric energy harvester with storage system*. *J Mech Sci Technol* 2020;34:4475–87. https://doi.org/10.1007/s12206-020-1008-4.

[9] Rui X, Li Y, Zheng X, Sha Z, Zeng Z. *Design and experimental study of a piezoelectric energy harvester in automotive spokes*. *J Phys D Appl Phys* 2019;52. https://doi.org/10.1088/1361-6463/ab2756.

[10] Horne J, Snowdon MM, Jia Y. *Using artificial gravity loaded nonlinear oscillators to harvest vibration within high g rotational systems*. *J Phys Conf Ser* 2018;1052. https://doi.org/10.1088/1742-6596/1052/1/012096.

[11] Rui X, Zeng Z, Li Y, Zhang Y, Yang Z, Huang X, et al. *Modeling and analysis of a rotational piezoelectric energy harvester with limiters*. *J Mech Sci Technol* 2019;33:5169–76. https://doi.org/10.1007/s12206-019-1006-6.

[12] Rui X, Zeng Z, Zhang Y, Li Y, Feng H, Yang Z. A *design method for low-frequency rotational piezoelectric energy harvesting in micro applications*. *Microsyst Technol* 2020;26:981–91. https://doi.org/10.1007/s00542-019-04628-4.

[13] Guo T, Xu Z, Huang L, Hu M, Jin L, Wang J. *Analytical Modeling and Performance Study of a Piezoelectric Laminated Annular Plate for Rotary Energy Harvesting*. *IEEE Access* 2020;8:214966–77. https://doi.org/10.1109/ACCESS.2020.3040197.

[14] Fang S, Wang S, Zhou S, Yang Z, Liao WH. *Exploiting the advantages of the centrifugal softening effect in rotational impact energy harvesting*. *Appl Phys Lett* 2020;116. https://doi.org/10.1063/1.5140060.

[15] Fang S, Wang S, Miao G, Zhou S, Yang Z, Mei X, et al. *Comprehensive theoretical and experimental investigation of the rotational impact energy harvester with the centrifugal softening effect*. *Nonlinear Dyn* 2020;101:123–52. https://doi.org/10.1007/s11071-020-05732-1.

[16] Gu L, Livermore C. *Compact passively self-tuning energy harvesting for rotating applications*. *Smart Mater Struct* 2012;21. https://doi.org/10.1088/0964-1726/21/1/015002.

[17] Gedeon D, Rupitsch SJ. D7.1 - *An Experimental Setup for Piezoelectric Cantilevered Vibration Energy Harvesters on a Rotating Drive Shaft* 2020:530–4. https://doi.org/10.5162/sensor2017/d7.1.

[18] Hsu JC, Tseng CT, Chen YS. *Analysis and experiment of self-frequency-tuning piezoelectric energy harvesters for rotational motion*. *Smart Mater Struct* 2014;23. https://doi.org/10.1088/0964-1726/23/7/075013.

[19] Fang S, Fu X, Du X, Liao WH. *A music-box-like extended rotational plucking energy harvester with multiple piezoelectric cantilevers*. *Appl Phys Lett* 2019;114:1–6. https://doi.org/10.1063/1.5098439.

[20] Khameneifar F, Arzanpour S, Moallem M. *A piezoelectric energy harvester for rotary motion applications: Design and experiments*. *IEEE/ASME Trans Mechatronics*2013;18:152734.https://doi.org/10.1109/TMECH.2012.2205266.

[21] Sadeqi S, Arzanpour S, Hajikolaei KH. *Broadening the Frequency Bandwidth* 2015;20:2085–94.

[22] Deng L, Jiang J, Zhang D, Zhou L, Fang Y. *Design and modeling a frequency self-tuning vibration energy harvester for rotational applications*. *Energy* 2021;235:121414. https://doi.org/10.1016/j.energy.2021.121414.

[23] Rui X, Zeng Z, Zhang Y, Li Y, Feng H, Huang X, et al. *Design and Experimental Investigation of a Self-Tuning Piezoelectric Energy Harvesting System for Intelligent Vehicle Wheels*. *IEEE Trans Veh Technol* 2020;69:1440–51. https://doi.org/10.1109/TVT.2019.2959616.

[24] Cooley CG. *ENERGY HARVESTING FROM THE VIBRATION AND ROTATION OF HOST SYSTEMS USING PIEZOELECTRIC DEVICES* 2019:1–6.

[25] Gu L, Livermore C. *Passive self-tuning energy harvester for extracting energy from rotational motion*. *Appl Phys Lett* 2010;97.

https://doi.org/10.1063/1.3481689.

[26] Wang YJ, Chuang TY, Lee C. *Resonant frequency self-tunable piezoelectric cantilevers for energy harvesting and disturbing torque absorbing*. Sensors *Actuators, A Phys* 2019;285:25–34. https://doi.org/10.1016/j.sna.2018.10.043.

[27] Machado SP, Febbo M, Ramírez JM, Gatti CD. *Rotational double-beam piezoelectric energy harvester impacting against a stop. J Sound Vib* 2020;469:115141. https://doi.org/10.1016/j.jsv.2019.115141.

[28] Machado SP, Febbo M, Gatti CD, Ramirez JM. *Non-resonant energy harvester with elastic constraínts for low rotating frequencies*. *J Phys Conf Ser* 2017;922. https://doi.org/10.1088/1742-6596/922/1/012009.

[29] Febbo M, Machado SP, Gatti CD, Ramirez JM. *An out-of-plane rotational energy harvesting system for low frequency environments*. *Energy Convers Manag* 2017;152:166–75. https://doi.org/10.1016/j.enconman.2017.09.042.

[30] Leinonen M, Palosaari J, Juuti J, Jantunen H. *Axle mounted piezoelectric energy harvester for continuous energy harvesting from rotation and vibration*. *WCCM* 2017 - 1st World Congr Cond Monit 2017 2017:1–10.

[31] Febbo M, Machado SP, Ramirez JM, Gatti CD. *A low frequency rotational energy harvesting system*. *J Phys Conf Ser* 2016;773. https://doi.org/10.1088/1742-6596/773/1/012058.

[32] Ramírez JM, Gatti CD, Machado SP, Febbo M. *A piezoelectric energy harvester for rotating environment using a linked E-shape multi-beam*. *Extrem Mech Lett* 2019;27:8–19. https://doi.org/10.1016/j.eml.2018.12.005.

[33] Yang L, Zhang H. *A wide-band piezoelectric energy harvester with adjustable frequency through rotating the angle of the jointed beam*. *Ferroelectrics* 2017;520:237–44. https://doi.org/10.1080/00150193.2016.1232108.

[34] Ramírez JM, Gatti CD, Machado SP, Febbo M. *An experimentally validated finite element formulation for modeling 3D rotational energy harvesters*. *Eng Struct* 2017;153:136–45. https://doi.org/10.1016/j.engstruct.2017.10.027.

[35] Febbo M, Machado SP. *Rotational multi-beam energy harvester with up conversion mechanism in an extremely low frequency scenario*.*Mech Syst SignalProcess*,2022;168:108737.https://doi.org/10.1016/j.ymssp.2021.108737.

[36] Mei X, Zhou S, Yang Z, Kaizuka T, Nakano K. *A tri-stable energy harvester in rotational motion: Modeling, theoretical analyses and experiments*. *J Sound Vib* 2020;469:115142. https://doi.org/10.1016/j.jsv.2019.115142.

[37] Zhang Y, Cai Y, Teng X, Zheng R, Nakano K. *Combining sustainable stochastic resonance with high-energy orbit oscillation to broaden rotational bandwidth of energy harvesting from tire.* e 2020;015011. https://doi.org/10.1063/1.5131429.

[38] Fang S, Wang S, Mei X, Zhou S, Yang Z, Liao WH. *A centrifugal softening*

impact energy harvester with the bistability using flextensional transducers for low rotational speeds. *SmartMaterStruct*2020;29.https://doi.org/10.1088/1361-665X/abad4f.

[39] Zou HX, Zhang W ming, Li WB, Wei KX, Gao QH, Peng ZK, et al. *Design and experimental investigation of a magnetically coupled vibration energy harvester using two inverted piezoelectric cantilever beams for rotational motion*.*EnergyConversManag*2017;148:13918.https://doi.org/10.1016/j.enconman.2017.07.05.

[40] Mei X, Zhou R, Fang S, Zhou S, Yang B, Nakano K. *Theoretical modeling and experimental validation of the centrifugal softening effect for high-efficiency energy harvesting in ultralow-frequency rotational motion*. *Mech SystSignalProcess*2021;152:107424.https://doi.org/10.1016/j.ymssp.2020.107424.

[41] Zhang Y, Cai Y, Teng X, Zheng R, Nakano K. *Combining sustainable stochastic resonance with high-energy orbit oscillation to broaden rotational bandwidth of energy harvesting from tire*. *AIP Adv* 2020;10. https://doi.org/10.1063/1.5131429.

[42] Zhang Y, Zheng R, Shimono K, Kaizuka T, Nakano K. *Effectiveness testing of a piezoelectric energy harvester for an automobile wheel using stochastic resonance*. *Sensors (Switzerland)* 2016;16. https://doi.org/10.3390/s16101727.

[43] Mei X, Zhou S, Yang B, Kaizuka T, Nakano K. *The Centrifugal Softening Effect*

*of an Inverse Nonlinear Energy Harvester in Low-frequency Rotational Motion for Enhancing Performance*2020:18.https://doi.org/10.1109/powermems49317.2019.41031604008.

[44] He L, Wang Z, Wu X, Zhang Z, Zhao D, Tian X. *Analysis and experiment of magnetic excitation cantilever-type piezoelectric energy harvesters for rotational motion*. *Smart Mater Struct* 2020;29. https://doi.org/10.1088/1361-665X/ab7f45.

[45] Lo YC, Chen CC, Shu YC, Lumentut MF. *Broadband piezoelectric energy harvesting induced by mixed resonant modes under magnetic plucking*. Smart *Mater Struct* 2021;30. https://doi.org/10.1088/1361-665X/ac1d8f.

[46] Zhang Y, Zheng R, Kaizuka T, Su D, Nakano K, Cartmell MP. *Broadband vibration energy harvesting by application of stochastic resonance from rotational environments*. *Eur Phys J Spec Top* 2015;224:2687–701. https://doi.org/10.1140/epjst/e2015-02583-7.

[47] Guo B, Chen Z, Cheng C, Yang Y. *Characteristics of a nonlinear rotating piezoelectric energy harvester under variable rotating speeds*. I*nt J Appl Electromagn Mech* 2015;47:411–23. https://doi.org/10.3233/JAE-140077.

[48] Zhang Y, Jin Y, Li Y. *Enhanced energy harvesting using time-delayed feedback control from random rotational environment*. *Phys D Nonlinear Phenom* 2021;422:132908. https://doi.org/10.1016/j.physd.2021.132908.

[49] Zhang Y, Zheng R, Nakano K, Cartmell MP. *Stabilising high energy orbit oscillations by the utilisation of centrifugal effects for rotating-tyre-induced energy harvesting*.*ApplPhysLett*2018;112:27.https://doi.org/10.1063/1.501997.

[50] Zhang Y, Jin Y. *Stochastic dynamics of a piezoelectric energy harvester with correlated colored noises from rotational environment*. *Nonlinear Dyn* 2019;98:501–15. https://doi.org/10.1007/s11071-019-05208-x.

[51] Mei X, Zhou S, Yang Z, Kaizuka T, Nakano K. *The benefits of an asymmetric tri-stable energy harvester in low-frequency rotational motion*. *Appl Phys Express* 2019;12. https://doi.org/10.7567/1882-0786/ab0b75.

[52] Forsberg G. *Piezoelectric energy harvesting using stochastic resonance in rotating systems* 2019.

[53] Wang S, Fan Y, Stroe D-I, Fernandez C, Yu C, Cao W, et al. *Battery state-of-power evaluation methods. Batter Syst Model* 2021:227–54. https://doi.org/10.1016/b978-0-323-90472-8.00004-4.

[54] Hopkins DC, Baltis T, Pitaress JM, Hazelmyer DR. *Extreme thermal transient stress analysis with pre-stress in a metal matrix composite power package*. *Proc - IMAPS Int Conf Exhib High Temp Electron* HiTEC 2012 2012:361–72. https://doi.org/10.4071/hitec-2012-tha25.

[55] Liu T, Xia X, Wu W, Yin C, Wang Y, Tian H, et al. *Experimental investigations for electric heating rotary stretch bending process of extruded Ti-6Al-4V alloy*

profile with T-section. *Procedia Eng* 2017;207:747–52. https://doi.org/10.1016/j.proeng.2017.10.823.

[56] Adams RD. *Measurement of the Mechanical Properties of a Carbon Reinforced Bismaleimide Over a Wide Range of Temperatures* 2005:29–34.

[57] Abdelkefi A, Yan Z, Hajj MR. *Temperature impact on the performance of galloping-based piezoaeroelastic energy harvesters*. *Smart Mater Struct* 2013;22. https://doi.org/10.1088/0964-1726/22/5/055026.

[58] Nguyen NT, Seo OS, Lee CA, Lee MG, Kim J hoon, Kim HY. *Mechanical behavior of AZ31B Mg alloy sheets under monotonic and cyclic loadings at room and moderately elevated temperatures*. *Materials (Basel)* 2014;7:1271–95. https://doi.org/10.3390/ma7021271.